Very High-Resolution Regional Climate Simulations over Scandinavia—Present Climate

OLE B. CHRISTENSEN AND JENS H. CHRISTENSEN

Danish Meteorological Institute, Copenhagen, Denmark

BENNERT MACHENHAUER AND MICHAEL BOTZET

Max Planck Institute for Meteorology, Hamburg, Germany

(Manuscript received 11 February 1997, in final form 7 October 1997)

ABSTRACT

The hydrological cycle on a regional scale is poorly represented with a present-day coarse resolution general circulation model (GCM). With a dynamical downscaling technique, in which a regional higher-resolution climate model (RCM) is nested into the GCM, this starts to become feasible. Here the authors go one step further with a double nesting approach, applying an RCM at 19-km horizontal resolution nested into an RCM at 57-km resolution over an area covering the Scandinavian Peninsula. A 9-yr-long time-slice simulation is performed with the driving boundary conditions taken from a fully coupled ocean–atmosphere GCM experiment, the recently completed ECHAM4/OPYC3 control simulation performed by the Max Planck Institute for Meteorology in Hamburg. With increasing resolution, local effects playing a significant role in the hydrological budget become better and better resolved and are more realistically simulated. It is found in particular that in mountainous regions the high-resolution simulation shows improvements in the simulation of hydrologically relevant fields such as runoff and snow cover. Also, the distribution of precipitation on different intensity classes is most realistically simulated in the high-resolution simulation. It does, however, inherit certain large-scale systematic errors from the driving GCM. In many cases these errors increase with increasing resolution. Model verification of near-surface temperature and precipitation is made using a new gridded climatology based on a high-density station network for the Scandinavian countries compiled for the present study. The simulated runoff is compared with observed data from Sweden extracted from a Swedish climatological atlas. These runoff data indicate that the precipitation analyses are underestimating the true precipitation by as much as 96% on an annual basis in the most mountainous region of Sweden. This fact as well as estimates of the underestimation in other areas of Scandinavia make the high-resolution RCM simulations appear more realistic.

1. Introduction

The representation of atmospheric and surface processes on a regional scale is treated in a simple way only in present atmospheric global circulation models (GCMs). The necessarily coarse resolution of this kind of model limits its skill with respect to simulation of fields depending on horizontally strongly variable local features. In particular, narrow mountain ridges, complex terrain in general, and complicated land–sea contrasts are absent or described in an insufficient way. This is reflected in the inability of GCMs, currently employing a spatial resolution of about 250 km, to simulate the accumulation and storage of water in the winter snowpack and its melting in the spring in a realistic way (Giorgi and Mearns 1991). To be able to give a reliable estimate of anthropogenic climate change relevant for impact studies, it is also essential to be able to simulate such parameters with credibility. The nesting approach with a high-resolution regional climate model (RCM) embedded into a GCM offers the possibility to reach this goal. However, even with a resolution increased to about 50 km, which is used in many RCMs (Giorgi 1990; Jones et al. 1995; Machenhauer et al. 1996; Christensen et al. 1997; Machenhauer et al. 1998), the resolution does not appear to be adequate to resolve the most complex terrains.

In this study we have applied a nesting in two steps to obtain a simulation at very high resolution. The finest resolution RCM, at a horizontal resolution of 19 km is driven by an RCM with a resolution of 57 km, which in turn is driven by a GCM that has a resolution of about 250 km (spectral T42). Experience from numerical weather prediction modeling shows that too big a difference in resolution between driving fields and an RCM gives numerical problems. Therefore the double nesting.

We focus on the Scandinavian Peninsula where many finescale details in the topography are responsible for the local climate. At the high resolution used here, local

Corresponding author address: Ole Christensen, Danish Meteorological Institute, Lyngbyvej 100, DK-2100 Copenhagen Ø, Denmark.
E-mail: bossing@dmi.dk

orographic features relevant for the snowpack and for precipitation start to become resolved.

In Fig. 1 the surface topography over Scandinavia may be compared at the three different model resolutions adopted here. Also shown is a station network of climatological rain gauges used for model validation. It is evident from this figure that the representation of mountains depends critically on the resolution. Note in particular the northernmost mountains appearing higher and narrower, and the generally much steeper slope of the terrain along the Norwegian mountains seen with 19-km resolution. The coarse GCM resolution hardly shows any slope of the mountains at all.

At first a 10-yr-long time-slice simulation with the 57-km RCM using boundaries from a coupled ocean—atmosphere GCM (CGCM) present-day climate simulation (Roeckner et al. 1996a) was performed at the Max Planck Institute (MPI). In the following analyses we disregard the data from the first year of the simulation in order to allow for a proper spinup of the model surface fields. Then the 19-km resolution simulation was performed at Danish Meteorological Institute (DMI) with 9 yr and 8 months of the 10-yr 57-km simulation as boundaries; again only the last 9 yr were saved and used. Corresponding $2 \times CO_2$ time-slice simulations based on boundary conditions from an MPI CGCM simulation with transiently increasing greenhouse gas concentrations have also been completed. The analysis of the resulting climate changes is the subject of Machenhauer et al. (1998). Along with several other RCM simulations over Europe an extensive assessment of the present simulations was also included in Machenhauer et al. (1998). Here we shall draw upon results from this assessment and extend it in a more detailed validation focusing on elements of the hydrological cycle over Scandinavia.

In section 5 we will verify the two RCM and the GCM present-day climate simulations against observations over Scandinavia. In this validation we will use data analyses of available station climatology data (1961–90) on the finest model grid. Simple approximative methods have been used to correct for station elevations different from the model orography.

The rest of this paper is organized in the following way. Section 2 gives information about the model system used and section 3 contains a description of the observations and the analysis technique applied. Section 4 describes the experimental setup. In section 5 we show the results and compare with observations. Finally, section 6 summarizes and concludes on the results.

2. Model description

a. The MPI CGCM

The atmospheric component of the MPI CGCM, ECHAM4, used in the present simulations is described thoroughly in Roeckner et al. (1996b). ECHAM4 is an Eulerian spectral model based on the primitive equations using a leapfrog, semi-implicit time-stepping scheme with weak time filter. Most prognostic variables, vorticity, divergence, and temperature in 19 hybrid-coordinate layers as well as the logarithm to the surface pressure are represented by spherical harmonics with a triangular truncation at wavenumber 42 (T42). This corresponds approximately to a horizontal resolution of 250 km in an equivalent gridpoint model. The water vapor and cloud water in ECHAM4 are represented in gridpoint space (the transform grid) only. These variables are advected using a semi-Lagrangian scheme (Williamson and Rasch 1994).

The physical parameterization of the ECHAM4 global model applies the radiation scheme of Morcrette (1991) with some modifications such as a consideration of additional greenhouse gases [methane, nitrous oxides, and 16 chlorofluorocarbons (CFCs)] and various types of aerosols, a revision of the water vapor continuum (Giorgetta and Wild 1996), and a revision of the single-scattering properties of cloud droplets and ice crystals and of the parameterization of their effective radii.

Full radiation calculations are done every 2 h during integration. This is done to balance the CPU demands on the radiation code relative to the other model components. The effective longwave emissivities and shortwave transmissivities are calculated and stored. These quantities are subsequently used for a quick update of the heating rates at the intermediate (20 min) time steps, accounting for changes in the solar angle and the vertical temperature profile only. Information on model cloud cover and liquid water content is used only at the *full* time steps.

An advanced parameterization for precipitation processes is adopted. Convection is described in the Tiedtke (1989) mass-flux formulation with modifications to the formulation of deep convection (Nordeng 1994). Liquid water in stratified clouds is a prognostic variable and treated according to the Sundqvist (1988) scheme with modifications according to Roeckner et al. (1992).

Land surface parameterization uses five temperature layers and one (bucket) moisture layer. Runoff is calculated within the Arno scheme (Dümenil and Todini 1988). The global dataset of fields of land surface parameters used in ECHAM4 (Claussen et al. 1994) is constructed from the major ecosystem complexes of Olson et al. (1983).

In the presence of a snowpack over land with a depth exceeding 9-m water equivalent, the surface in the grid point is considered to be covered with ice—that is, to be a glacier—and soil temperature equations are solved with the characteristics of ice. In case of the snowpack being less thick than 0.025-m water equivalent, the equations are solved assuming bare soil. In the intermediate case an additional heat conduction equation is solved for the snow temperature in order to extrapolate the temperature relevant for the middle of the snow layer to a radiative temperature at its surface.

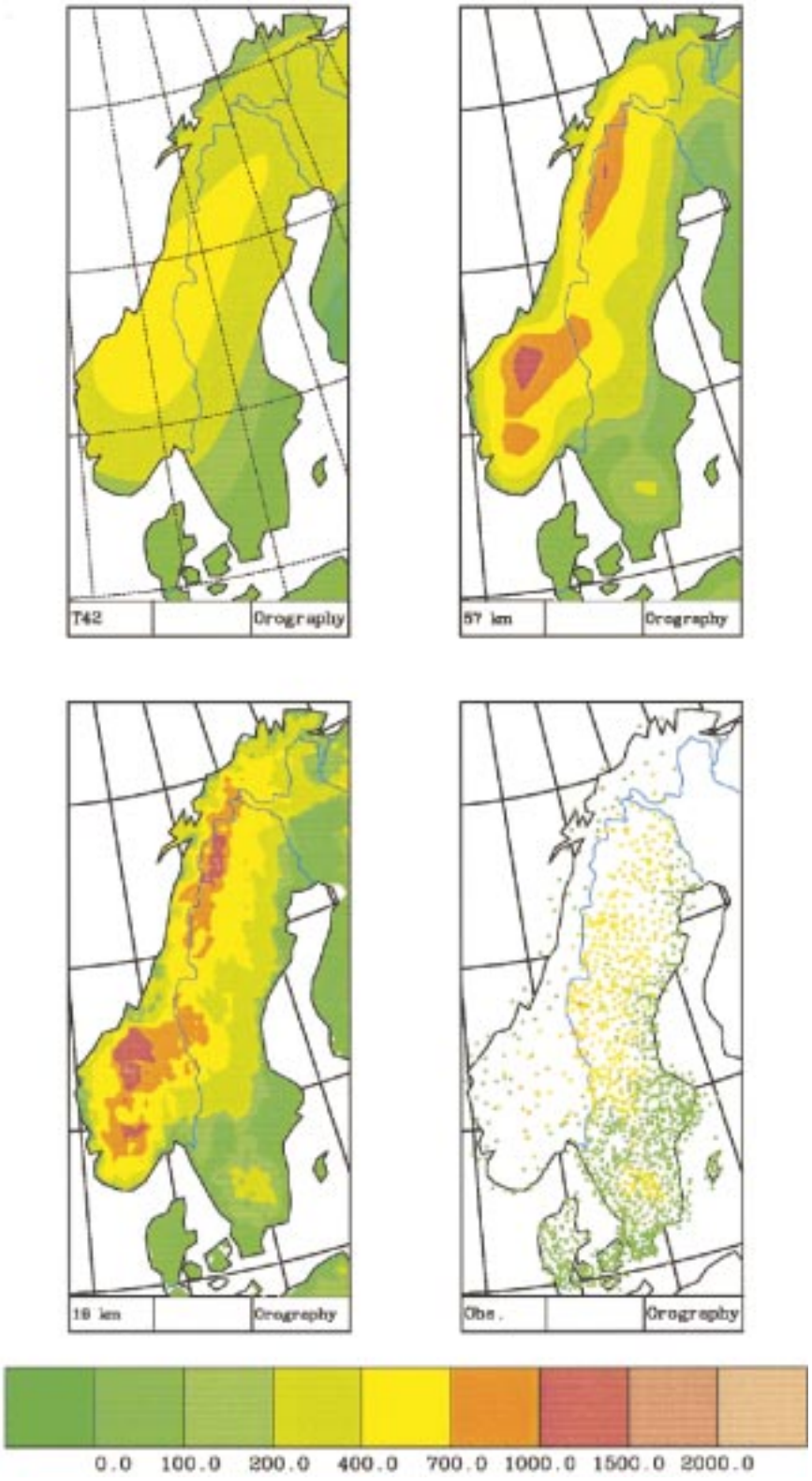

FIG. 1. Surface topography (m) over Scandinavia at various resolutions: T42 GCM, 57 km RCM, and 19 km RCM. Lower-right panel shows station elevations of the rain gauge network (see section 4).

The oceanic model component OPYC3 is described in Oberhuber (1993). It consists of three submodels for the interior ocean, the surface mixed layer, and the sea ice, respectively. The model for the interior ocean employs the primitive equations in a form of the conservation laws for momentum, mass, and salinity at 11 isopycnal layers. The mixed layer model computes entrainment and detrainment rates into and out of the layer according to budget equations for the turbulent kinetic and mean potential energy. The sea-ice model solves equations for ice momentum, ice and snow thickness, and their concentration. The thermodynamic part consists of a prognostic computation of the temperature profile.

b. The HIRHAM4 medium- and high-resolution RCMs

The regional climate model HIRHAM4 employed in this study is based on the HIRLAM[1] short-range weather prediction model (Källén 1996). To make a model that is suitable for long climate integrations, the more advanced physical parameterization of the MPI climate model ECHAM4 has been incorporated into the model. By choosing a physical parameterization package consistent with that used in the driving GCM, one reason for the development of large differences over the lateral boundary zones is eliminated. A detailed description of the combined model, called HIRHAM4, can be found elsewhere (Christensen et al. 1996). Some of the important characteristics of the model are summarized below.

HIRHAM4 is a standard primitive-equation Eulerian staggered gridpoint model with a prognostic cloud water equation. The time-stepping scheme is similar to that used in the ECHAM4 model, except for the advection of liquid water, which is calculated using a simple forward-upstream scheme. The model has a variable number of vertical hybrid levels, at present 19 levels similar to those adopted in ECHAM4. We operate with a lateral boundary relaxation zone, currently 10 points wide, following Kållberg and Gibson (1977) with a quasi-exponential relaxation function for most prognostic variables. Moisture and cloud water, however, are relaxed according to a so-called inflow–outflow scheme where only the value on the edge of the area is modified: if the flow is directed out of the integration domain, a value extrapolated from upstream quantities is applied at the model levels, otherwise the boundary value is taken from the coarser-resolution field.

As in ECHAM4, surface mean orography and variances are obtained from a U.S. Navy database, which has a spatial resolution of $\frac{1}{6}^\circ \times \frac{1}{6}^\circ$. Other surface fields are based upon Claussen et al. (1994).

A linear fourth-order horizontal diffusion scheme is applied, but in mountainous regions it is switched off for temperature and humidity in order to avoid spurious mixing of air masses from different pressure levels causing unphysical precipitation. To prevent ''gridpoint storms'' a weak smoothing of the tendencies of humidity is applied prior to the call to the physics (Sass 1994). To avoid reflection of gravity waves from the upper boundary, a five-layer sponge filter (Shapiro 1970) is applied for temperature, wind, and specific humidity.

A few modifications in the physical parameterization of the ECHAM4 model have been performed. A retuning of parameters related to cloud formation has been performed to handle the higher resolutions. These are partly based on previous sensitivity experiments made with ECHAM4 but also on such experiments made with the HIRHAM4 model itself.

Sea ice is treated in a way adopted from the OPYC3 ocean model (Oberhuber 1992), where the heat conduction equations are solved for sea ice as well as for the snow on top of the sea ice.

3. Experimental setup

a. The MPI CGCM climate simulation

The coupling procedure used in the ECHAM4–OPYC3 coupled present-day climate simulations is described in Roeckner et al. (1996a). Prior to the coupling, the OPYC3 ocean component has been spun up for about 1000 yr by prescribing a combination of observed and ECHAM4-simulated fluxes. After a subsequent 100-yr coupled spinup simulation, flux corrections constant in time are applied to the fluxes of heat and freshwater in order to avoid a large climate drift when the restoring boundary conditions are replaced completely by the fluxes computed in ECHAM4.

b. The RCM climate simulations

The MPI CGCM climate experiment was initiated at year 90 of the 100-yr coupled spinup run, and 6-h output for a 10-yr time-slice—years 151–160—were prepared for boundary conditions to the RCM simulations.

As already mentioned, the nesting is performed in two steps. First, the CGCM output is used as boundary conditions for a HIRHAM4 integration with an average resolution of 57 km in a domain covering Europe and the North Atlantic, hereafter referred to as the DKH area. With this choice of area, a comparison of the climate of the whole of Europe is possible between the RCM and the GCM (Machenhauer et al. 1998). The DKH domain is the full domain shown in Fig. 2. The output of this simulation drives the integration of HIRHAM4 with an average resolution of 19 km in an area covering Scandinavia and the North Sea, hereafter referred to as the SCN area (see Fig. 2).

[1] High Resolution Limited Area Model; developed by the national meteorological institutes in Denmark, Finland, Holland, Iceland, Ireland, Norway, and Sweden, later also in cooperation with France and Spain.

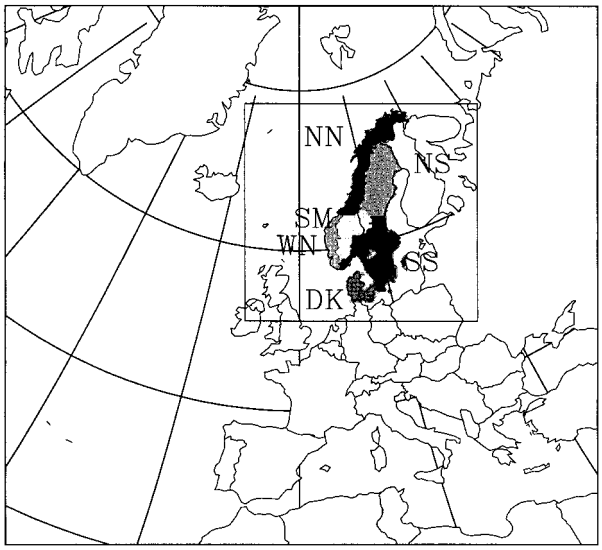

FIG. 2. The integration area of the present 19-km simulation (SCN) shown within the 57-km resolution domain (DKH). The different shadings outline the subareas used [WN: western Norway, NN: northern Norway, NS: northern Sweden, SM: southern mountains, SS: southern Sweden (see section 5a)].

Problems related to mismatch between driving fields and model fields in the boundary relaxation zone are serious only on the outflow boundary where the weather systems leave the RCM, as the flow here has had time to deviate from the driving flow during the time the weather systems spend inside the model domain. This gives rise to unphysical convergence and divergence near the outflow relaxation zone. Since the flow in general is westerly or southwesterly, we do not see any serious boundary errors in Scandinavia, the present area of interest, which is at a sufficient distance from the eastern boundaries.

To get boundary conditions for the 57-km HIRHAM4 simulation, the GCM prognostic fields of surface pressure, temperature, wind, and specific humidity are linearly interpolated in time and space to the DKH grid. The sea surface temperature (hereafter SST), sea-ice concentration and thickness, and snow depth on sea ice are horizontally interpolated to the DKH grid every 24 h. In the SCN simulation a similar procedure is adopted with the lateral boundaries taken from the DKH simulation.

The DKH grid has dimensions 110×100, and a time step of 5 min is applied; the SCN area has dimensions 130×121 and the time step is 2 min. Thus, especially the SCN integration is demanding in terms of computational costs. It has been feasible to perform the SCN integration on the NEC SX-4 supercomputer of DMI. The DKH simulation was performed by the MPI on the Cray C90 of the Deutsches Klimarechenzentrum (DKRZ).

4. Validation data

In this work we focus on the ability of the models to simulate hydrological budgets; that is, we validate climatological means of near-surface parameters like air temperature, precipitation, snow cover, and runoff. As the resolution of the SCN simulations is much higher than it is usual for climate simulations, the standard databases for verification—for example, Jäger (1983); Legates and Willmott (1990), and even the more recent one Hulme et al. (1995) that was used in Machenhauer et al. (1998)—were considered to be too crude for a proper validation of the model performance.

Therefore we have established a special high-resolution station database of monthly climatological means (1961–90) for surface air temperature and precipitation in Scandinavia (Denmark, Norway, and Sweden). In Fig. 1 the distribution of the stations of the combined dataset of rain gauges is shown. A color code is used to highlight elevations. The density of stations with temperature records is thinner, but resembles the distribution of rain gauges shown for Norway. The dataset has been produced from printed tables issued by the national Swedish and Norwegian meteorological services (Alexandersson et al. 1991; DNMI 1994) and digitized data obtained from DMI.

a. Analysis method

To transform station data to model gridpoint values, we apply a successive correction method (Bergthorsson and Doos 1955). In this method point observations are transformed into a regular lattice field through iterative corrections as outlined in the following.

An analysis increment at a grid point is found by averaging differences between observation values Q_k at observation points k and the previous analysis field $\mathbf{P}^{(n-1)}$ using a weight function w defined for observations within a certain characteristic radius R_n. For each iteration n, the value of R_n is reduced. At grid point i, the surrounding stations k are assigned weights:

$$W_{ik}^{(n)} = \frac{w^{(n)}(r_{ik})}{\sum_l w^{(n)}(r_{il})}, \qquad w^{(n)}(r) = \frac{R_n^2 - r^2}{R_n^2 + r^2}, \quad (1)$$

where r_{ik} is the distance between observation point k and lattice point i.

Thus, the procedure for an analysis iteration is the following:

1) Linear interpolation of the previous analysis field $\mathbf{P}^{(n-1)}$ to points of observation, leading to a vector of deviations at the observation sites $\Delta\mathbf{Q}^{(n)} = \mathbf{Q} - \mathbf{L}\mathbf{P}^{(n-1)}$, where $\mathbf{Q}$ is the vector of observations, $\mathbf{L}$ is the linear interpolation matrix that transforms grid values to values at the observation points, and $\mathbf{P}^{(n-1)}$ is the vector of previous analysis values at grid points at iteration $n - 1$.
2) Computation of the analysis increments $\Delta\mathbf{P}^{(n)}$ as

TABLE 1. Lapse rates based on the dataset from Hulme et al. (1995).

Month	Jan	Feb	Mar	Apr	May	Jun	Jul	Aug	Sep	Oct	Nov	Dec
Climatological lapse rate (10^{-3} K m^{-1})	5.01	5.66	6.01	5.97	5.88	5.84	5.53	5.22	5.33	5.24	5.21	4.94

weighted averages of the deviations $\Delta\mathbf{Q}^{(n)}$ located at the observation sites using the weight matrix $\mathbf{W}^{(n)}$, so that

$$\mathbf{P}^{(n)} = \mathbf{P}^{(n-1)} + \mathbf{W}^{(n)}\Delta\mathbf{Q}^{(n)} = (1 - \mathbf{W}^{(n)}\mathbf{L})\mathbf{P}^{(n-1)} + \mathbf{W}^{(n)}\mathbf{Q}. \quad (2)$$

In the analyses presented in this work, we have used four iterations with radii $R_n = 200$, 100, 40, and 15 km. The analysis method is quite robust with respect to the specific choice of R_n; too many iterations can, however, give problems in areas with a low density of observations, for example, where the distance between observation points is larger than one or more of the R_n values.

The distribution of observations is somewhat inhomogeneous with the station density in Norway being much lower than in Denmark and Sweden. To make an analysis that does not let single stations dominate surrounding areas entirely in regions with a low density of observations, ideally one should have a sequence of characteristic radii depending locally on station density. As a poor man's way of doing this, we have introduced a cutoff maximal weight $\mathbb{W}_{\max} = 0.7$. An iteration will be skipped for a grid point if one station has a relative weight $\mathbb{W}_{ik}^{(n)} > \mathbb{W}_{\max}$. Since the nearest station to a grid point becomes increasingly important with decreasing R_n, this simply means that the total number of iterations depends on the local density of observations.

For temperature, observations were first reduced to mean sea level (MSL) applying a lapse rate that depends on the season. The lapse rates used were calculated in Machenhauer et al. (1998) from the climatological data of Hulme et al. (1995), which gives temperature values at three different elevations at each grid point. These climatological lapse rates are given in Table 1. They vary between the extremes 6.0 and 4.9 K km^{-1} in March and December, respectively. Since temperature varies significantly between coastal regions and the interior of a country, we have introduced a discrimination of coastal stations such that temperature observations at coastal coordinates corresponding to a fraction of land in the model grid below 0.4 are excluded from the analysis, which we apply only to model land points (fraction of land >0.5). This procedure reduces the number of Norwegian stations used in the analysis since quite a large number of these are situated on minor islands off the Norwegian main coast (cf. Fig. 1). This reduction amounts to 15% of the total number of stations, or 23% of the Norwegian stations. The analyses of the temperatures reduced to MSL are compared to simulated surface air temperatures also reduced to MSL, again using the climatological lapse rates.

In the case of precipitation we do not have a simple dependency on elevation. The correlation between altitude and precipitation depends on surface slope orientation, wind direction, and many other factors. We have restricted ourselves to taking elevation into account by discriminating observations taken at an elevation very different from the model orography. This is done by modifying the weights to $\tilde{w}^{(n)}(r_{ik}) = \exp(-|h_i - h_k|/h_c)w^{(n)}(r_{ik})$, where h are elevations and h_c is a characteristic scale. We have found 500 m to be a reasonable value. For precipitation we have not considered it necessary to discriminate against coastal stations.

b. Other validation fields

To get beyond a simple validation of just climatological means of precipitation and surface air temperature is very difficult, since the data for other variables are usually not readily available. These data are often only available in the form of maps in atlases or similar publications produced in the individual countries. For the Scandinavian Peninsula some information is provided in a Norwegian (Aune et al. 1993) and a Swedish (Raab and Vedin 1995) national atlas. In the same atlases the climatological means of surface air temperature and precipitation are also provided, hence allowing for a consistency check of the analyses we have made of these parameters. By a visual comparison of the maps in the national atlases with the similar maps produced using our analysis of the station data, we generally obtain a reasonable agreement. However, in the mountainous regions the fields differ. We ascribe this primarily to the different surface topography used in the analyses.

For Norway and Sweden we have extracted information from these atlases on precipitation intensity classes, and for Sweden also on runoff data. For Denmark the precipitation statistics have been made available in digital form. For snow cover we have adopted the 1° climatology from Foster and Davy (1988), which we interpolated to the high-resolution model grid.

To describe the general circulation over Europe generated by the present models we shall also consider analyses of mean sea level pressure (MSLP). As in Machenhauer et al. (1998) these will be compared to a climatology based on 14 yr of operational analyses from the European Centre for Medium-Range Weather Forecasts (ECMWF).

5. Results

a. Basic parameters in the validation

In Figs. 3–6 we present the seasonally averaged values of the ECMWF climatology of MSLP, the standard

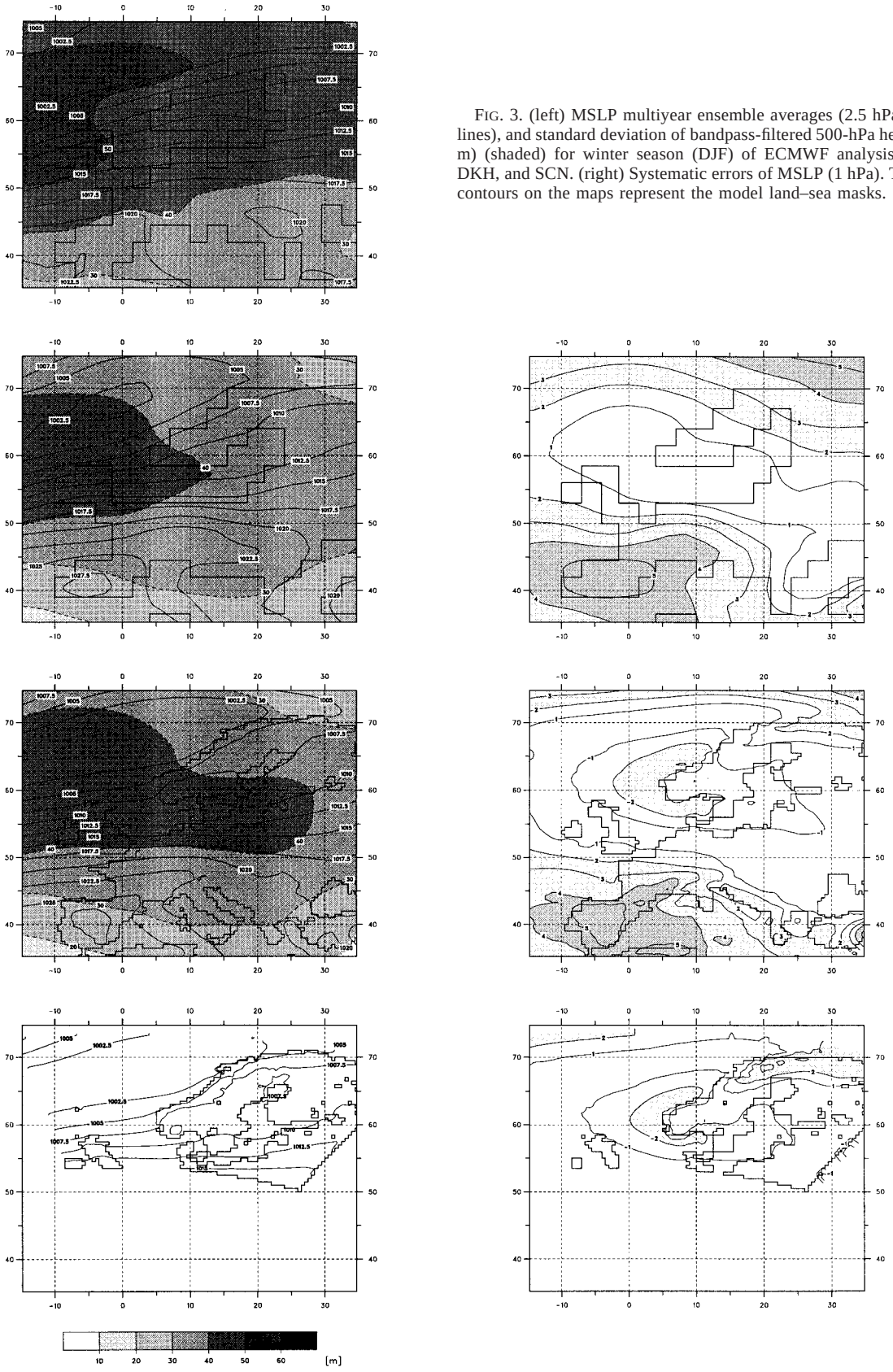

FIG. 3. (left) MSLP multiyear ensemble averages (2.5 hPa) (solid lines), and standard deviation of bandpass-filtered 500-hPa height (10 m) (shaded) for winter season (DJF) of ECMWF analysis, GCM, DKH, and SCN. (right) Systematic errors of MSLP (1 hPa). The land contours on the maps represent the model land–sea masks.

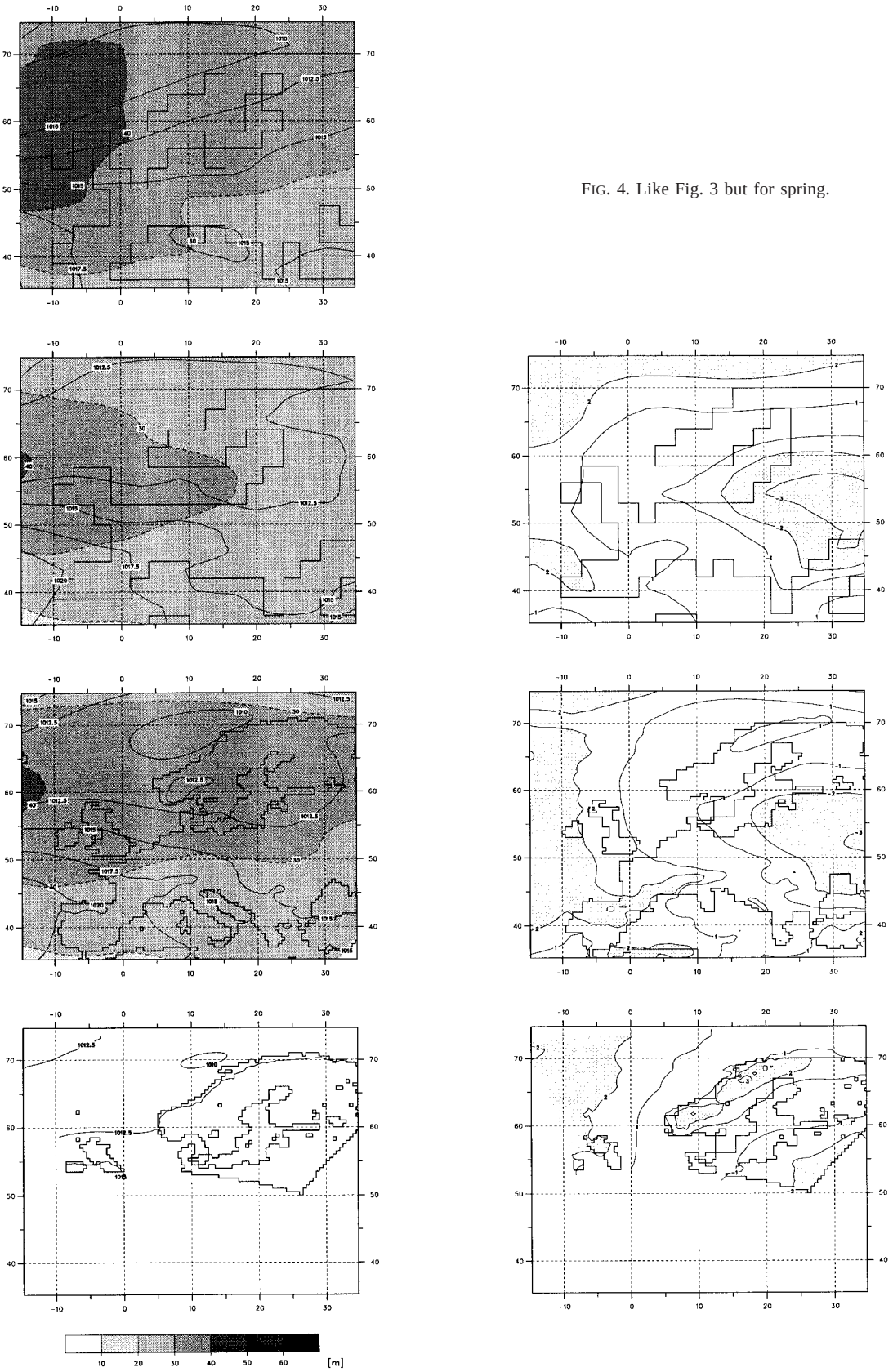

FIG. 4. Like Fig. 3 but for spring.

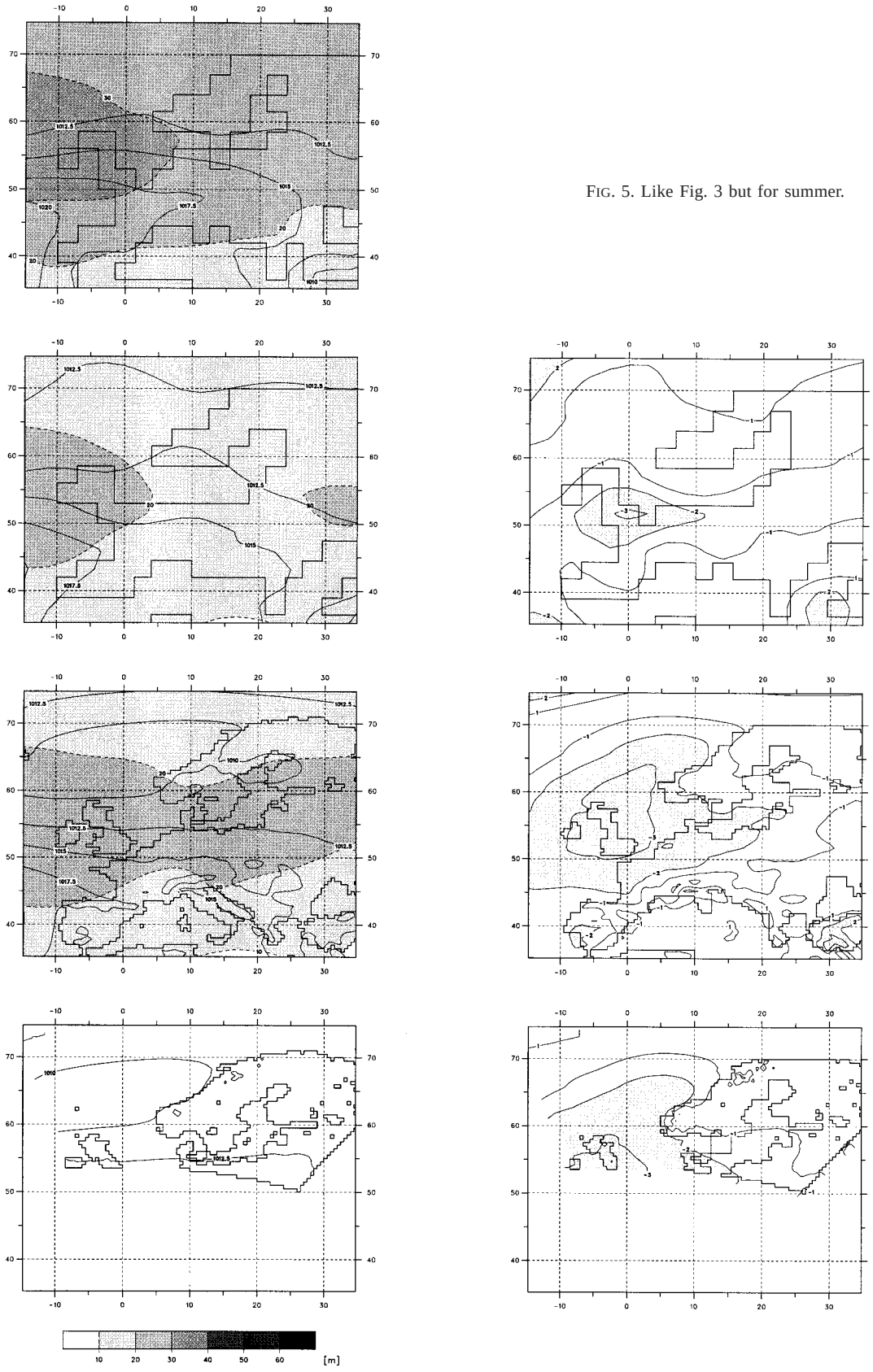

FIG. 5. Like Fig. 3 but for summer.

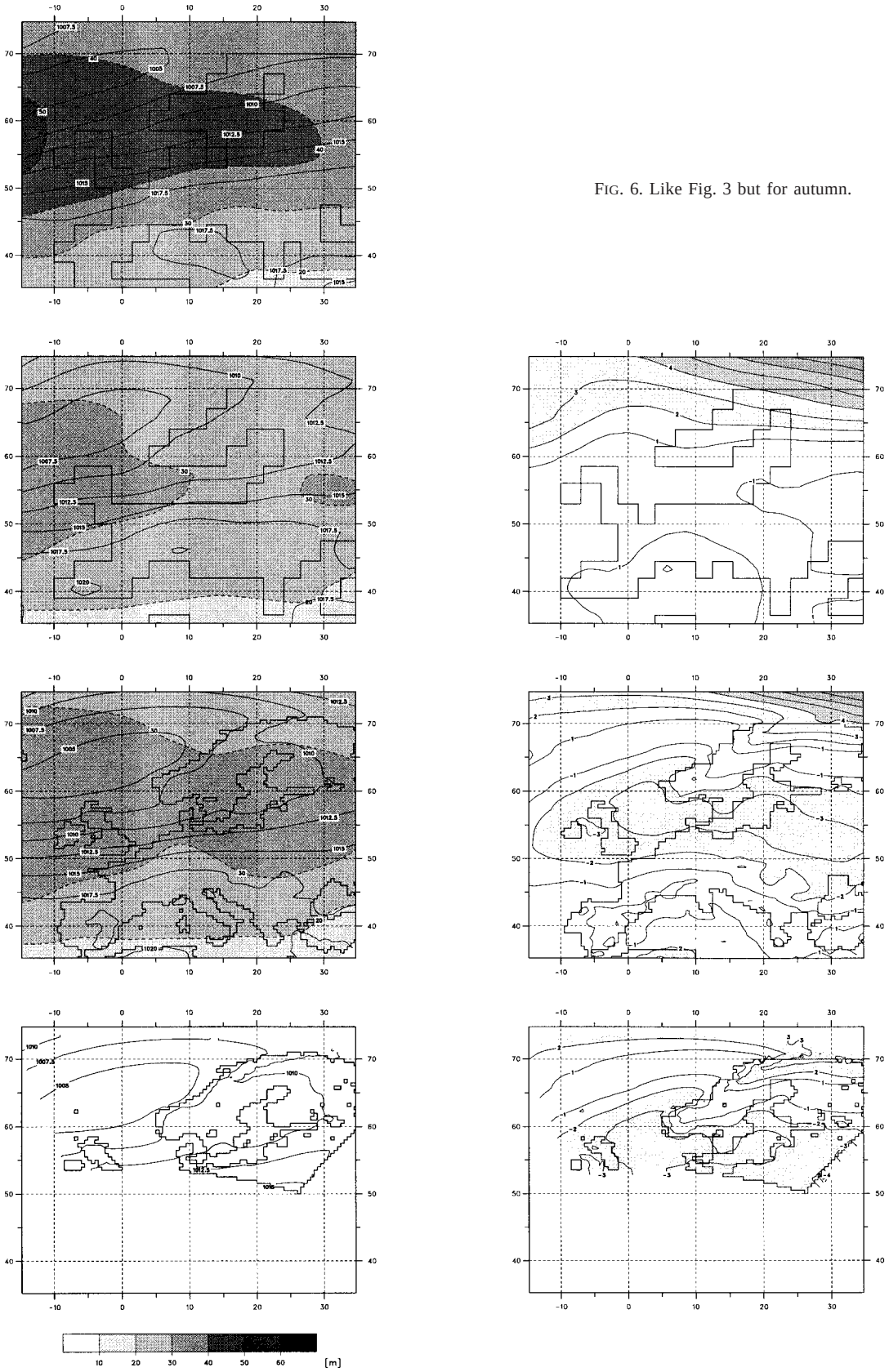

FIG. 6. Like Fig. 3 but for autumn.

deviation of band-pass filtered (2.5–6 days) 500-hPa heights (Blackmon 1976), and the model systematic errors in MSLP.

Following Machenhauer et al. (1998) we present the maps of the systematic errors in MSLP because of their inherent information about errors in the general circulation, that is, the mean horizontal and vertical motions and superimposed eddy motions of the lower troposphere. The general circulation over Europe is decisive for the time-averaged surface air temperature and precipitation fields. Systematic errors in the circulation patterns will therefore to a large extent explain the biases in the precipitation and temperature patterns presented in Figs. 7 and 8.

An area with too high pressure indicates too much subsidence and hence reduced precipitation and generally also reduced cloudiness. When the cloudiness is reduced the surface air temperature will typically be reduced in winter and increased in summer due to changes in the local radiation balance. An area with a too low pressure on the other hand indicates excessive rising motions and hence increased precipitation and probably also increased cloudiness.

Between the regions of too high pressure and those of too low pressure in the MSLP bias maps, we find areas of relatively large pressure bias gradients. Assuming gradient flow, with frictional modifications in the planetary boundary layer, these are areas with erroneous horizontal advection of heat and moisture by the mean flow in the lower troposphere. When the erroneous advection is enforcing (or weakening) an advection from the Atlantic, it intensifies (or weakens) the advection of moist air, which typically leads to increased (or decreased) cloudiness and precipitation. The erroneous advection of Atlantic air usually also transports heat, which, along with erroneous cloudiness, may lead to errors in the surface air temperature. Such temperature biases may be large, positive during winter and negative during summer.

When situated in connection with the North Atlantic storm track an area of too low pressure indicates increased extratropical cyclone activity in the form of too deep, too slowly moving, or too slowly filling low pressure systems. In either case such increased activity will lead to increased precipitation, created not only by large-scale ascending motion but also by convective precipitation. It will also result in increased transport of heat and moisture in the meridional direction. Such an eddy heat and moisture transport will tend to create positive precipitation biases and positive or negative temperature biases to the north of the cyclone tracks. As an example, if in winter excessive heat and moisture is supplied in the southern part of a belt of too low pressure due to excessive advection from the Atlantic, then the increased cyclone activity will result in an increased eddy transport of heat and moisture toward the north and thus establish positive temperature and precipitation biases in the north.

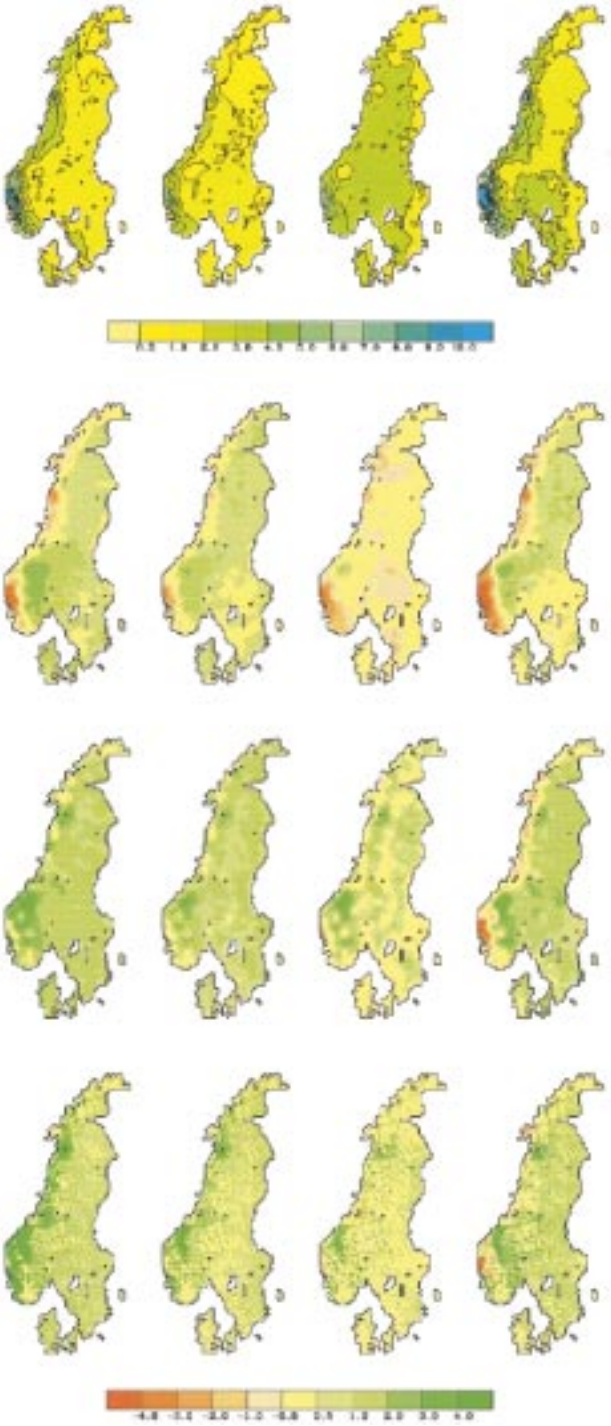

FIG. 7. (upper row) Analyzed precipitation (mm day^{-1}) for winter, spring, summer, and autumn. (lower rows) Model biases relative to the DMI analysis (mm day^{-1}); GCM (row 2), DKH (row 3), and SCN (row 4).

The positions of the cyclone tracks in reality and as simulated are indicated by the fields of standard deviation of band-pass-filtered 500-hPa heights, which are superimposed on the MSLP fields in Figs. 3–6. Here

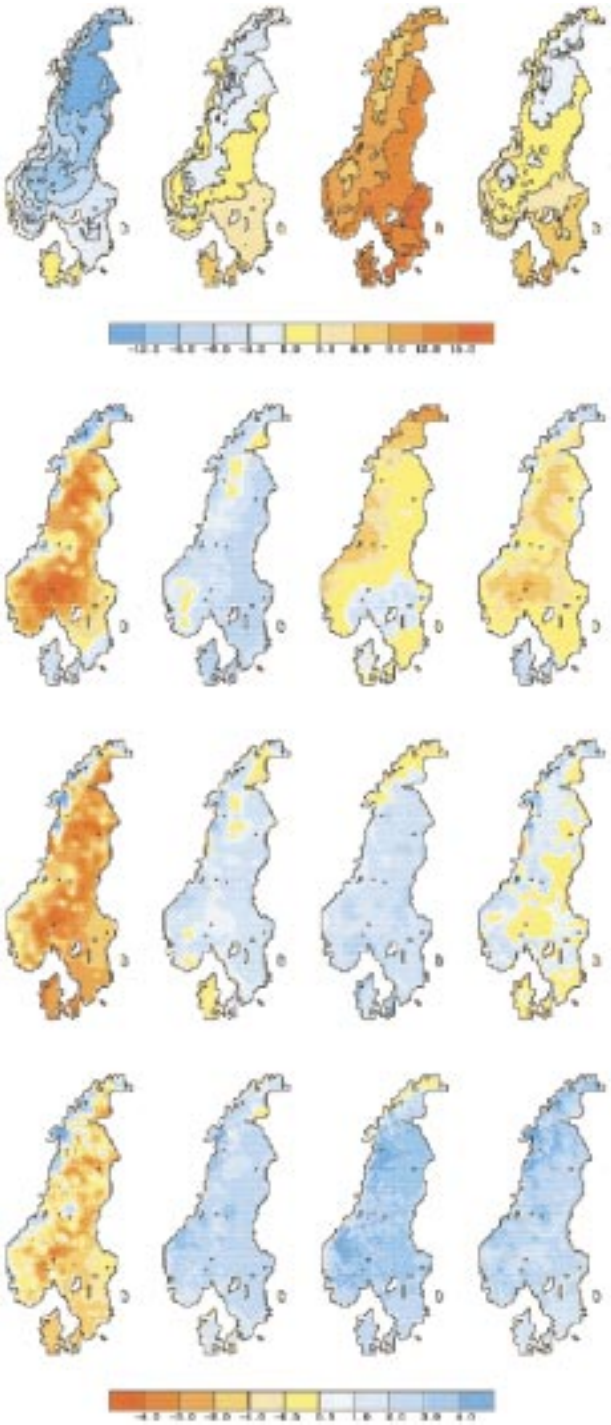

FIG. 8. (upper row) Analyzed 2-m temperature (°C) for winter, spring, summer, and autumn. (lower rows). Model biases relative to the DMI analysis (°C), GCM (row 2), DKH (row 3), and SCN (row 4). simulations.

we interpret this standard deviation as a storm track parameter. A belt of high values of this parameter shows the preferential position of the cyclone tracks.

The seasonal mean biases of the SSTs around Europe in the CGCM simulation, which are used in the regional simulations too, are shown in Machenhauer et al. (1998). Biases are relative to the climatology determined from 10 yr of AMIP [Atmospheric Model Intercomparison Project (Gates 1992)] data. Around Europe a pronounced seasonal variation of the biases is found, with extremes around Denmark and in the Mediterranean numerically up to between 3 and 5 K, and even larger in the Black Sea. The simulated SSTs are too warm in winter and too cold in summer. That such large-amplitude seasonal SST bias variations can develop in the CGCM simulation must be due to the flux corrections being independent of season. It seems obvious that they must influence the simulations of temperatures and precipitation significantly over Europe and thus add another source of errors to those mentioned above.

On the SCN grid we have defined a set of subareas—that is, climatologically distinct regions that we will refer to later on in our validation. The subareas are shown in Fig. 2. We have based the selection of the subareas partly on our analyzed fields of precipitation and similar maps in Aune et al. (1993) and Raab and Vedin (1995) and partly on orographical criteria. Subarea WN represents the wet upslopes (under typical westerly flow condition) of western Norway west of the main inland mountain areas. To the north, the WN subarea does not extend beyond 63°N. Subarea NN, mainly northern Norway, represents the upslope side of the northern part of the Scandinavian mountains. This subarea is separated from the lee side (subarea NS, mainly Northern Sweden) by the orographical summits in the east–west direction. Subarea SM (Southern Mountains) defined in Fig. 2 is representative of the inland mountain areas, which have mean grid cell altitudes down to 700 m on the western side and down to 500 m on its eastern side. Subarea SS (mainly in southern Sweden) is representative of the low land part of southern Scandinavia, except for Denmark, which we have chosen to be the separate subarea DK. The separation between subareas WN and SS is determined by the summit criterion mentioned above.

Note that we have not used the national border between Norway and Sweden to separate the subareas. Thus, for instance NS includes parts of Norway, and NN includes parts of Sweden.

We have interpolated quantities from the GCM and the DKH grids to the SCN grid and used these interpolated values for integrations over the subareas. Since the topography varies a lot between the experiments (cf. Fig. 1), we have applied the following procedure to obtain quantities for the two lower-resolution experiments: considering land-point values from the lower resolution grid as pseudoobservations, we perform an analysis of these as described in section 4a with SCN as a target grid. Furthermore, as part of the analysis procedure temperatures are reduced to MSL taking into account the climatological lapse rates so that differences

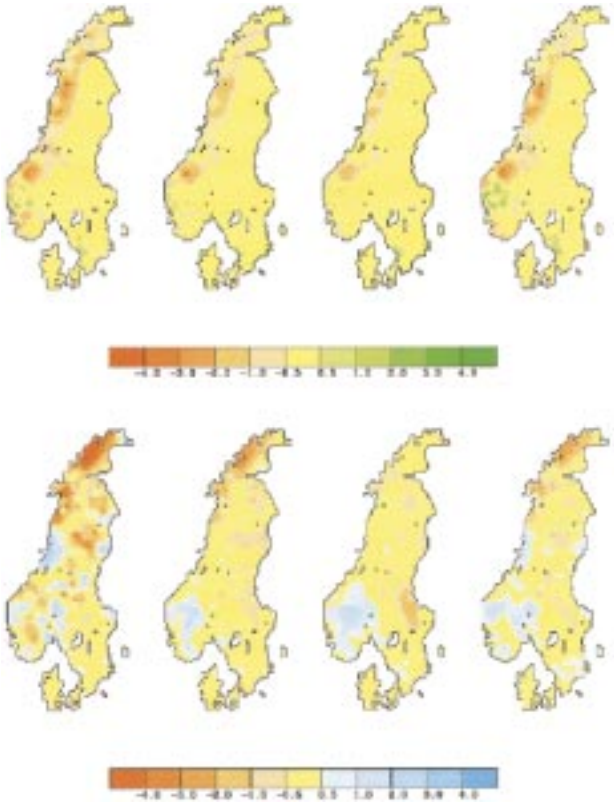

FIG. 9. Difference between the DMI and the CRU analyses (DMI–CRU). (upper row) Precipitation (mm day^{-1}) for winter, spring, summer, and autumn. (lower row) Temperature (°C), same sequence of seasons.

due to variations with altitude of climatological temperatures are eliminated.

b. Validation of the gridded surface climatology

We have compared the analyses of surface air temperature and precipitation described above (hereafter the DMI analyses) to those of Hulme et al. (1995), in the following referred to as the CRU (Climate Research Unit) analyses. In the case of temperature, the CRU analyses are based on daily minimum and maximum temperatures and the mean temperature is defined as a simple midpoint of these, whereas our analyses are based on reported daily mean temperatures. Furthermore, the present dataset is based on more stations than used in the CRU climatology, especially in Sweden and Denmark. The analyses by Hulme et al. (1995) differ from ours by including the elevation as a predictor of the climate variable. For each parameter the CRU data in each grid cell is available for a minimum, an area mean, and a maximum value of the surface topography. We have compared our results only with the data determined at the CRU mean orography. This mean orography is similar to the orography used in the DKH simulation (e.g., Fig. 1).

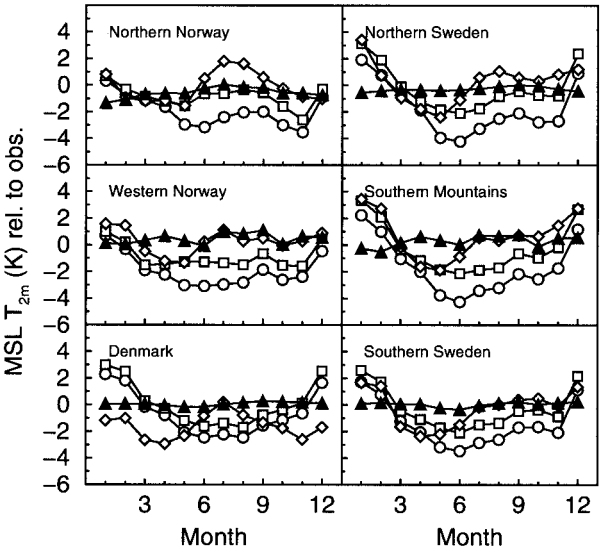

FIG. 10. Average MSL air temperature biases for six subareas of Scandinavia (Fig. 2) and three different simulations relative to the DMI analysis (circles: SCN, squares: DKH, diamonds: GCM, filled triangles: CRU climatology).

We compare the analyses on the SCN grid, since our station network is dense enough over Sweden and Denmark to provide a reasonably adequate climatology on that scale. Hence, to illustrate the major differences in the two analyses Fig. 9 shows on the SCN grid the difference fields of precipitation and 2-m temperature reduced to MSL (see above) for the four seasons; winter (DJF), spring (MAM), summer (JJA), and autumn (SON), respectively. We have interpolated the CRU climatology horizontally by treating the data as observations using the successive correction method described above. We note two main differences. First, our analysis of temperature during winter is substantially warmer (exceeding 4°C) in the northern part of the area, except in the extreme northeast where it is slightly colder. A similar pattern is found in the two transitional seasons, but with somewhat lower amounts. Over the southern Norwegian mountains our analysis is slightly colder in all seasons but winter. Second, our precipitation analysis shows substantially lower values throughout the year along the northern mountains, although most pronounced for winter and autumn. We note that in the areas where these main differences are seen, there are very few observations (Fig. 1) and furthermore it is in mountainous areas where the analyses must depend strongly on the different procedures used to account for orography. In addition, we note minor differences over Sweden for both temperature and precipitation, which we must attribute to our denser station network.

The quantitative effects on the subarea mean values of the differences between the DMI and the CRU analyses may be seen in Figs. 10 and 11. In the former it is seen that the temperature differences between the two analyses are small compared to the biases of the model

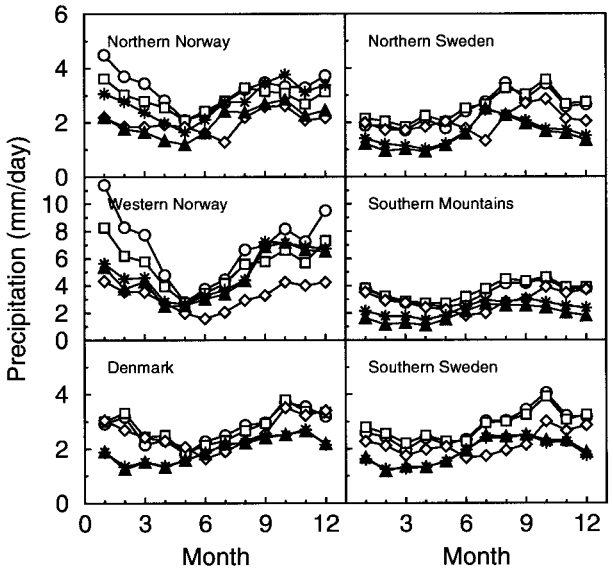

FIG. 11. Average precipitation for six subareas of Scandinavia (Fig. 2) and three different simulations (circles: SCN, squares: DKH, diamonds: GCM, filled triangles: DMI climatology, asterisks: CRU climatology). Note that the middle row has a different scale.

simulations also shown. Generally the differences are smaller than 1K with the exception of the somewhat larger difference in winter in NN. Fig. 11 shows that also the precipitation differences are generally small compared with the model biases, in all cases smaller than 1 mm day^{-1}. As we also saw in Fig. 9 the largest differences between the two analyses are in the mountain areas NN and SM, where the differences in winter come close to 1 mm day^{-1}. Here the density of observations are about equal in the two analyses and we assume that the CRU analysis is the most correct one with respect to the way variations with elevation are taken into account. The CRU analysis is the one closest to the RCM simulated precipitation. The mean seasonal biases of the CRU analyses with respect to the DMI analyses are included in Tables 2 and 3.

Both the DMI and the CRU analyses suffer from errors in the observations. The raw rain gauge observations are systematically underestimating the actual precipitation due to strong wind effects and wetting loss. The dominating wind effect is especially strong for precipitation falling as snow, of course strongest for unsheltered gauges, for high wind speeds, and for low temperatures. For Denmark the corrections of the 1931–60 normals (Allerup and Madsen 1980) for unsheltered gauges were estimated to be 15% and 28% in the summer and winter seasons, respectively. For gauges that are moderately sheltered, which is typical for the Danish stations, the corresponding numbers are 12% and 21%. The corrections for the total annual precipitation were estimated to be 16% for moderately sheltered, and 20% for unsheltered gauges. These estimates give probably somewhat too small corrections as indicated by newer studies (Vejen 1996). Estimates of the corrections for Norway and Sweden are not available, but they are expected to be larger than for Denmark, as more of the

TABLE 2. Observed surface air temperature reduced to MSL (°C). Temperature bias (°C) relative to the DMI analysis for subareas (Fig. 2).

Season	Source	Western Norway	Northern Norway	Northern Sweden	Southern mountains	Southern Sweden	Denmark
Winter	Observation	−0.7	−6.8	−9.8	−4.9	−3.5	0.6
	CRU bias	0.2	−1.1	−0.5	−0.1	0.2	0.1
	GCM bias	1.3	−0.4	1.8	3.0	1.5	−1.3
	DKH bias	0.6	0.0	2.5	2.7	2.2	2.7
	SCN bias	0.0	−0.4	1.2	1.5	1.2	1.9
Spring	Observation	5.4	1.1	1.3	4.1	4.9	6.4
	CRU bias	0.4	−0.6	−0.4	0.4	0.0	0.0
	GCM bias	−1.0	−1.3	−1.7	−1.2	−2.1	−2.6
	DKH bias	−1.4	−1.2	−1.1	−1.1	−1.1	−0.4
	SCN bias	−2.4	−1.9	−2.2	−2.3	−2.1	−1.0
Summer	Observation	13.9	12.2	13.8	14.6	15.5	15.4
	CRU bias	0.6	−0.1	−0.2	0.5	−0.1	0.0
	GCM bias	0.5	1.3	0.2	0.0	−0.5	−0.5
	DKH bias	−1.4	−0.5	−1.6	−1.9	−1.7	−1.6
	SCN bias	−3.0	−2.5	−3.3	−3.6	−3.0	−2.4
Autumn	Observation	6.8	2.7	2.1	5.0	6.4	9.0
	CRU bias	0.6	−0.5	−0.1	0.4	0.1	0.2
	GCM bias	0.2	−0.2	0.6	1.0	0.3	−1.9
	DKH bias	−1.6	−1.6	−0.7	−0.6	−0.6	−0.3
	SCN bias	−2.3	−2.8	−2.5	−2.2	−1.8	−1.1
Total	Observation	6.4	2.3	1.9	4.7	5.8	7.8
	CRU bias	0.5	−0.6	−0.3	0.3	0.0	0.1
	GCM bias	0.3	−0.1	0.3	0.7	−0.2	−1.6
	DKH bias	−‘1.0	−0.8	−0.2	−0.2	−0.3	0.1
	SCN bias	−1.8	−1.9	−1.7	−1.7	−1.4	−0.6

TABLE 3. Observed precipitation (mm day^{-1}) and relative precipitation bias with respect to the DMI analysis for subareas (Fig. 2) in percentages.

Season	Source	Western Norway	Northern Norway	Northern Sweden	Southern mountains	Southern Sweden	Denmark
Winter	Observation	5.2	2.1	1.2	1.5	1.6	1.8
	CRU bias	8	44	17	37	−3	1
	GCM bias	−22	−3	63	123	53	71
	DKH bias	39	53	97	140	81	81
	SCN bias	87	86	81	136	73	74
Spring	Observation	3.1	1.4	1.0	1.3	1.4	1.5
	CRU bias	8	43	8	31	−2	0
	GCM bias	−12	34	79	90	38	53
	DKH bias	34	77	96	114	65	53
	SCN bias	64	99	80	101	55	42
Summer	Observation	3.6	2.1	2.1	2.4	2.3	2.1
	CRU bias	6	19	0	12	−1	0
	GCM bias	−39	−21	−16	−10	−22	−7
	DKH bias	23	32	33	57	20	14
	SCN bias	38	29	35	41	22	23
Autumn	Observation	6.9	2.6	1.7	2.3	2.4	2.5
	CRU bias	3	33	6	21	−2	1
	GCM bias	−44	−6	47	49	9	23
	DKH bias	−12	15	78	85	44	33
	SCN bias	−8	30	69	78	50	35
Total	Observation	4.7	2.1	1.5	1.9	1.9	2.0
	CRU bias	6	34	7	23	−2	1
	GCM bias	−31	1	33	52	34	32
	DKH bias	16	39	68	92	48	28
	SCN bias	39	56	61	81	46	51

precipitation is falling as snow, and there are more unsheltered gauges, especially in mountain areas where also the wind speeds become high. For Sweden we have made estimates (section 5d) of the corrections on the annual precipitation based on estimates of the real precipitation from analyses of runoff and estimated evaporation. For the parts of subareas NN, NS, SM, and SS inside Sweden these estimates give corrections of 96%, 43%, 51%, and 35%, respectively. Included in these corrections are also errors due to shortcomings of the analysis. One such error is caused by the dominance of low-level stations in mountain areas and an insufficient way of taking into account the increase of precipitation intensities with altitude. The CRU analysis takes this variation of intensities with altitude into account so that the difference between the two analyses (the CRU bias) may be taken as an estimate of this error in the DMI analyses. As seen in Table 3 on a seasonal and an annual basis, these biases are relatively small for all subareas except for SM and NN.

c. Validation of temperature and precipitation

To do a quantitative comparison between models and observations, we show in Figs. 10–14 the variation of monthly averages over the subareas described previously. In Fig. 10 we present temperature biases—that is, area-averaged temperatures reduced to MSL with the lapse rates of Table 1—and subtracted the area averages of the DMI analysis. As discussed in section 5b we also show biases for the alternative CRU climatology. For reference we show in addition in Table 2 observed temperatures and biases for the four seasons. In Fig. 11 we show total precipitation for the three simulations and the two climatologies. In Table 3 we list observed precipitation values for the four seasons as well as CRU and model biases in percent of the DMI analysis.

1) WINTER

In the present GCM simulation a center of too high pressure is situated over the Iberian Peninsula (Fig. 3). Between this center and the center of too high pressure in the northeast we see a belt of relatively low pressure. The systematic MSLP errors in the DKH and SCN simulations are very similar to those in the GCM, except that in both simulations the pressure has decreased further in the belt of relatively low pressure. This is a typical effect of higher resolution when going from a GCM to a regional model (Machenhauer et al. 1996; Machenhauer et al. 1998). Also here we see a decrease of pressure between the GCM and the DKH simulation. However, between the DKH and the SCN simulations we see a slight increase in the center of too low pressure. In both RCM simulations the too low pressure indicates too strong cyclone activity in these belts, in particular in the DKH simulation. The small-scale ridge of too high pressure over Scandinavia and the troughs on each side of it increase with increasing resolution. This ridge–trough error pattern is created by the westerly flow, crossing the mountain chain. Its increase with resolution, due to the increase in altitude of the mountain chain

with resolution, is seen in all seasons. Similar patterns are seen in other regional climate simulations (Machenhauer et al. 1998). We know that the ECMWF analyses we have used are smoothed somewhat (they are spectrally truncated to the T42 resolution), and employ a too simplified procedure in the reduction to MSL. Hence, it seems likely that these orographical waves are not errors.

We also note here that the CGCM simulated seasonal SSTs are generally too warm relative to climatological SSTs, with biases exceeding 3 K near Denmark. Exceptions are a too cold northern part of the Baltic Sea and areas with negative biases to the northwest of the SCN domain (Machenhauer et al. 1998).

In the belt of too low pressure we find positive precipitation and temperature biases (Figs. 7 and 8 and Tables 2 and 3). The biases in the northern part of the belt of too low pressure on the eastern side of the Scandinavian mountains (Sweden) can be explained by the northward eddy heat and moisture transport due to the enhanced cyclonic activity and the advection by the mean error flow of relatively moist and warm Atlantic air around the center of too low pressure. Here the generally too high SSTs will tend to increase these biases except near the northern Baltic Sea where they are reduced due to the negative SST bias there. We note that when going from the DKH to the SCN simulation these areas experience a cooling and decreasing precipitation in agreement with the decrease in cyclone activity as indicated by the increase of pressure in the belt of too low pressure. It should be noted that the MSLP bias pattern to the north (Fig. 3) in all three simulations shows that the westerlies are weakened. This should imply dry and cold biases over land. The moistening and warming mechanisms discussed above seem to be dominant, however.

With the increasing resolution from the GCM to the SCN simulation we see (Fig. 11 and Table 3) a monotonic increase in precipitation over subareas NN and WN. A similar variation with resolution was found in Machenhauer et al. (1996).

As mentioned earlier, our analyses underestimate the precipitation at the upslopes and tops of mountains, mainly because the observations underestimate the amounts of snow. It is difficult to say how much, but in winter more than 40% may not be unrealistic in the WN and NN subareas, also because of the discrepancy between model orography and station elevation (see the CRU biases in Table 3). The GCM simulation (biases of −22% and −3%) is therefore clearly underestimating the precipitation, whereas the DKH (39% and 53%) and even the SCN (87% and 86%) simulation may be realistic. Thus, our results do indicate an improvement in orographical precipitation with increasing resolution, which apparently is explained by the increasing realism of the mountains with increasing resolution when, as here, the bias in the cross-mountain flow is relatively small. An increasing tendency for subsidence with increasing resolution in the lea of the mountains can be inferred from Fig. 12, which shows the cloud cover over the six subareas. In the winter months a weak but monotonic decrease in the cloudiness with increasing resolution is seen for the subareas on the lee side, south and east of the mountains—that is, SM, NS, SS, and even DK.

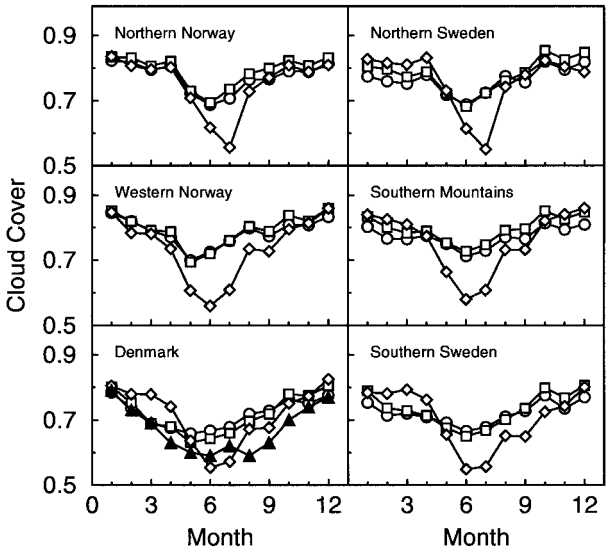

FIG. 12. Average cloud cover for six subareas of Scandinavia (Fig. 2) and three different simulations (circles: SCN, squares: DKH, diamonds: GCM, black triangles for Denmark: observations).

Similar monotonic increases, and thus improvements, in precipitation with increasing resolution are seen in these westernmost subareas in the other seasons, except for NN in summer where a slight decrease is seen going from DKH to SCN.

For western Norway we also see a monotonic decrease of temperature with increasing resolution from the GCM to the SCN simulations. This is also the case in the other seasons. The only explanation we can think of is connected with the eddy heat transport by the traveling extratropical cyclones. For the WN subarea the Scandinavian mountains must shelter against the northward heat transport connected with cyclones moving south of Norway, whereas cold air advection from the Norwegian Sea on the western side of the cyclones can easily reach the area. The sheltering effect of the mountains must increase with increasing resolution due to the increasing height of the mountains.

2) SPRING

The systematic MSLP error pattern of the SCN and DKH simulations is rather similar to that of the GCM simulation (Fig. 4), except for the orographically induced waves.

A center of too low pressure over eastern and central Europe indicates increased cyclone activity, which explains the enhanced precipitation seen (Figs. 7, 11, and

Table 3) in all subareas, except in the GCM on the western slope of the Norwegian mountains. The reduced precipitation there in the GCM is explained by the reduced westerlies. The precipitation is increased monotonically with resolution in subareas WN and NN, which is explained as for the winter season, whereas it increases slightly in the rest of the subareas to a maximum in DKH, then further decreases slightly from DKH to SCN. As in the other seasons the largest bias is found in SM, where the uncorrected bias is 114% in spring in DKH.

The temperature biases (Figs. 8, 10, and Table 2) are negative in all subareas and for all three models. The biases are explained by reduced advection from the Atlantic where the SSTs are higher than the land surface air temperatures. Around the Baltic Sea the negative biases are enhanced due to the negative SST biases there (up to 3°C too cold in the northern part). As explained previously the temperature biases in the subarea WN decrease monotonically with resolution. In subarea WN we find the numerical maximum bias for the season in SCN, −2.4°C. In the remaining subareas the temperature biases increase from the GCM to a numerical minimum in DKH and then they decrease again from DKH to SCN. This may be connected with the fact that all of these subareas have maximum precipitation bias in DKH. The larger release of latent heat may have increased the temperature.

An important question is why the negative biases increase numerically from DKH to SCN. This cannot be explained by changes in the mean advection or by the eddy transport by cyclones (Fig. 4). From Fig. 10 it is apparent that the difference between the biases in DKH and SCN increases with time during the spring season in all subareas. We see also that the differences remain large throughout the summer and autumn seasons. This indicates that the explanation has to do with the general seasonal heating of the land. We think that the lower temperatures in SCN can be explained by a more efficient exchange of the heat between land and sea by land–sea breeze systems. In SCN such systems are much better resolved and it seems reasonable to assume that their transport of the too cold air from the ocean to the land is more efficient than in DKH—the sea breeze is stronger than the land breeze. Perhaps the resulting cooling of the surface in SCN causes the reduction in the convective precipitation compared to DKH.

3) SUMMER

The GCM MSLP error field shows a belt of too low pressure across Europe with a center over the southern United Kingdom (Fig. 5). In both RCM simulations the negative bias center over the United Kingdom has expanded, mainly northward. In the GCM, Scandinavia is situated in the region of reduced westerlies north of the belt of too low pressure. This leads to a general reduction of precipitation and a warming as the Atlantic is colder than land this time of the year (Figs. 7 and 8). The SSTs of the CGCM are generally too cold with biases down to −5.0 K near Denmark (Machenhauer et al. 1998). Obviously the large negative SST biases around Europe must contribute to the reduction of the land temperatures in all three model simulations. In the GCM simulation they have reduced the positive temperature biases in Scandinavia and even lead to a cooling over Southern Sweden and Denmark (Fig. 8). In the area of too strong westerlies south and southeast of the pressure bias center over the United Kingdom, positive precipitation and negative temperature biases are to be found in the GCM (not shown) due to enhanced advection from the Atlantic. This is the case also in the RCM simulations but here the cold and moist air is advected by the eddy transport due to enhanced cyclone activity and the error mean flow in and around the more northerly center over England (Fig. 5), giving positive precipitation and negative temperature biases also over the Scandinavian Peninsula (Fig. 8).

The simulated precipitation amounts increase from the GCM to the DKH simulation to moderate positive subarea biases (Table 3). The absolute maximum in percent for the season is 57% in DKH, again in the subarea WN. These increases are caused by the change in MSLP bias pattern (or general circulation) as described above. For subarea WN the bias increase further from DKH to SCN, which was explained previously by the additional increase in steepness of the mountain slopes. In the rest of the subareas the precipitation either increases or decreases slightly in agreement with the fact that the MSLP bias patterns in DKH and SCN in Fig. 5 are quite similar.

All the simulated subarea temperatures decrease monotonically with resolution from GCM to the SCN simulation, the largest bias being −3.6 K in SCN in subarea SM. The changes from the GCM to the DKH simulation are explained by the changes in the general circulation and the effects of the steeper orography as mentioned above. It is seen in Fig. 12 that the changes in circulation are accompanied by rather large increases from GCM to DKH in cloud cover in all subareas. We note that for Denmark, where we have observations available, the evidence seems to be that the real world is somewhere between the two sets of simulations. This is in agreement with the negative precipitation bias in the GCM and the positive one in DKH in subarea DK. This increase in cloud cover in all subareas has contributed to the decreases in temperature. The further decrease in temperature from DKH to SCN may be explained by a more efficient transport by land–sea breeze systems of cold air from the much too cold ocean. Such systems may even have contributed to the cooling in DKH. As in the spring season it seems likely that the cooling of the land surface resulting from this land–sea breeze has reduced the convective precipitation. We see in some of the subareas a reduction in precipitation from DKH to SCN. The others in which there is a slight

TABLE 4. Frequencies of precipitation intensity classes for subareas (Fig. 2) in days/yr^{-1}.

Intensity	Source	Western Norway	Northern Norway	Northern Sweden	Southern mountains	Southern Sweden	Denmark
Dry	Observation	150	154	191	188	197	197
below 0.1 mm day^{-1}	GCM	39	57	52	34	39	46
	DKH	46	53	51	37	65	74
	SCN	61	80	74	61	82	81
Light	Observation	46	66	67	59	52	45
0.1–1.0 mm day^{-1}	GCM	92	119	128	100	141	113
	DKH	71	106	109	85	100	92
	SCN	71	100	115	103	104	102
Medium	Observation	103	115	93	98	95	106
1–10 mm day^{-1}	GCM	205	177	172	208	167	184
	DKH	177	178	182	203	171	170
	SCN	148	149	152	163	148	153
Heavy	Observation	66	30	14	20	21	17
above 10 mm day^{-1}	GCM	24	7	8	18	13	17
	DKH	66	23	18	35	24	24
	SCN	80	31	19	33	26	24

increase may indicate the dominance of a too efficient release of precipitation in the SCN simulation.

Even during summer a certain underestimation of the analyzed precipitation amounts must be expected due to strong wind effects and wetting loss. The underestimation in our analyses due to the altitude variation of precipitation intensities seems to be smallest in the present season as indicated by the fact that during summer the two analyses are less discrepant in the mountains than for the other seasons (Fig. 11 and Table 3).

4) AUTUMN

In all three simulations we see a belt of too low pressure (Fig. 6) aligned east–west, deepest in the RCM simulations. As usual, east of the Scandinavian mountains inside and north of the belt of too low pressure the precipitation biases are positive. This is explained by the enhanced cyclone activity and the excess advection from the Atlantic south of the belt of too low pressure. As this is deepest in the RCM simulations the biases are largest there. Over Scandinavia, north of the belt of too low pressure, the error flow from the east—that is, reduced westerlies—may explain the negative precipitation biases on the western slopes of the mountains.

The precipitation in subarea WN increases monotonically with increasing resolution, ending with an uncorrected bias of −8% in SCN. This is clearly an underestimation considering the assumed underestimation of the analyzed values. In all the subareas the largest changes due to resolution are found going from the GCM to DKH. Compared to these, the changes in going from DKH to SCN are small and seemingly random in agreement with the similarity of the error flow of both simulations. The maximum uncorrected precipitation bias found is 85% in DKH for subarea SM.

In the autumn the SSTs are normally warmer than the land surface. However, the biases in the North Sea and Baltic Sea are negative for the first part of the season, so there the SSTs actually used are probably colder than the land. In the Atlantic the SST biases are positive during the whole season. Hence, advected air from the Atlantic is generally warmer than the land surface. Thus, the enhanced advection from the Atlantic, south of the belt of too low pressure, and the excess eddy heat transport to the north due to enhanced cyclone activity is heating most of the eastern part of Scandinavia. This process dominates in the GCM simulation (Fig. 8). On the other hand, north of the too low pressure belt the mean error flow is westward. Thus the westerlies are reduced, which implies a cooling of Scandinavia. Apparently, in the DKH and even more so in the SCN simulation this cooling process dominates. Additional support to this finding is the fact that the strength of the mean error flow over Scandinavia increases from the GCM to the RCMs (Fig. 6). In Table 2 it is seen that the temperature decreases further with increasing resolution from DKH to SCN in all subareas The decrease in temperature from DKH to SCN in subarea WN is explained the same way as for the summer. As it is difficult to see any other reasons for this decrease in the remaining subareas, we again suggest that a more efficient land–sea breeze system in SCN is responsible for the transport of too cold air from the surrounding seas, at least in the first part of the season.

In this season the maximum temperature bias, −2.8 K, is found in SCN in the subarea NN.

d. Validation of other hydrological fields

Having made the validation of the basic climate parameters, temperature, and precipitation over Scandinavia, we are ready to validate some key parameters in the hydrological balance.

1) PRECIPITATION FREQUENCY

In Table 4 we have compiled information about observed precipitation frequencies in different classes of

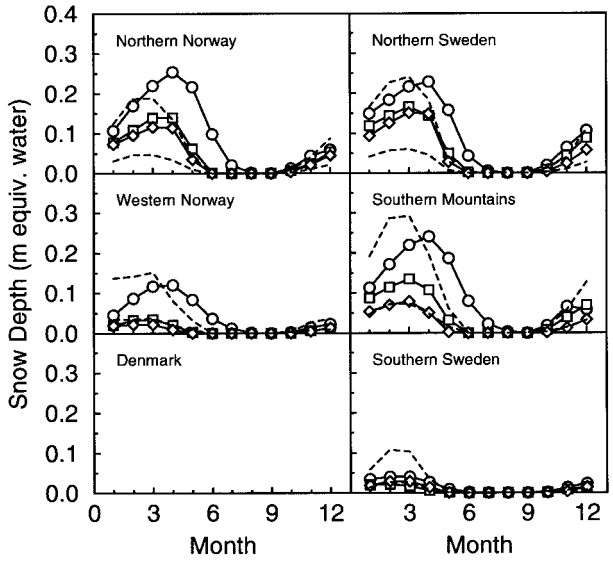

FIG. 13. Average snow depth for six subareas of Scandinavia and three different simulations [circles: SCN, squares: DKH, diamonds: GCM, dashed lines: observations from Foster and Davy (1988) with snowmass densities of 400 kg m^{-3} and 100 kg m^{-3}, respectively (see Table 5)]. In the SCN simulation snow is accumulating through the 9 yr of simulation because some glaciers are forming. Here we have subtracted the annual minimum from the values.

intensities for the subareas on an annual basis. This information is based on Aune et al. (1993), Raab and Vedin (1995), and data from DMI. Apart from the large spread in total observed precipitation amounts (Table 3), we see there is also a considerable spread in precipitation frequencies among the different subareas. Some parts of Norway are experiencing 215 day yr^{-1} with precipitation above 0.1 mm day^{-1}, whereas for Denmark the number of rainy days does not exceed 168. In the higher intensity regime we notice that the wet part of Norway has an expectation of 66 days with heavy precipitation (more than 10 mm day^{-1}), whereas such events are rather rare in northern Sweden, not exceeding 14 day yr^{-1}. The distribution on frequency classes of the simulated precipitation is also shown in the table.

The models have far too few dry days. This problem is improving somewhat with increasing resolution, although there is still a large gap to the observed numbers even for SCN.

For light precipitation (0.1–1.0 mm day^{-1}) all three models have too high a frequency. DKH and SCN are very similar and come closest to the observations. The frequencies simulated by both RCMs are still between 34% and 104% higher than observed.

For medium intensities (1.0–10.0 mm day^{-1}) the simulated intensities are again too large, but here the GCM and DKH models are close (except for subarea WN), whereas the SCN in all cases has a substantially lower frequency. These values are in better agreement with the observed values, although still between 30% and 83% higher than observed.

TABLE 5. Mass density of different types of snow from Raab and Vedin (1995).

Snow density	
Snow type	kg m^{-3}
Very light snow	<30
Newly fallen dry snow	30–100
Newly fallen wet snow	100–200
Wind-packed snow	200
Late winter packed snow	200–300
Snow in late spring during melting	400

Finally, the frequency of simulated heavy precipitation is much larger in the RCMs than in the GCM. In most subareas the RCMs are quite similar, with deviations less 29% from the observed values, except in WN, where SCN has a much higher value. In two subareas, SM and DK, the GCM is closer to the observed. That the frequency of heavy precipitation in the RCMs is substantially larger than in the GCM could be explained by a more realistic orographic lifting of air and by these models ability to develop deep low pressure systems.

For all three classes of precipitation intensities the GCM simulation is clearly inferior. For light precipitation the RCMs seem equally good although with far too high numbers. The SCN gives in all subareas the most realistic frequencies of the large class of medium intensity precipitation, although again too large. In the highest class, the SCN has the highest values, which in most cases also are too high compared to the observed values. However, the observed frequencies of heavy precipitation are probably underestimated just as the total precipitation amounts. Thus, even for heavy precipitation the SCN may give the most realistic results. The overprediction of low-intensity precipitation frequency seems to be a common problem in atmospheric models (Mearns et al. 1995).

2) SNOW COVER

In Fig. 13 we show the seasonal variation of the simulated snow cover in equivalent meters of water averaged over the six subdomains of Fig. 2. In this figure we also show observed values obtained by interpolating snow depth data from Foster and Davy (1988) to the SCN grid, according to the analysis procedure outlined in section 4a, and averaging these data for each of the areas in concern. The observational data are provided on a $1° \times 1°$ grid. We have converted the observed snow depth to equivalent meters of water, the same units that are used in the simulations. The two curves shown for each subarea represent the snowpack using snow densities corresponding to newly fallen snow (100 kg m^{-3}) and melting snow (400 kg m^{-3}), respectively, see Table 5. The real ''observed'' equivalent water depth should be something between the two curves, approaching the value for newly fallen snow in the beginning of

the winter season and approaching the curve for melting snow in late spring.

For the SCN simulation there is a problem in representing the snow cover like this. There are mountain peaks with a snow depth that increases from year to year, effectively building up glaciers. These points should be excluded from the average; in order to try to accomplish this in a simple way, we have for the SCN simulation for each subarea subtracted the smallest monthly value from all averages in Fig. 13.

The Foster and Davy (1988) data are mainly based on low-altitude measurements. Hence, the data will be biased and systematically underestimate the actual snow coverage in mountainous regions. This bias in the observations also explains why snow is shown to be absent from June to September in all areas, even in the mountainous subareas NN and SM. This is obviously not correct. Thus, in the following we present observations of runoff, which show that a substantial melting takes place in the summer season in the high mountains in northern Sweden near the border to Norway. As most of this runoff can be explained only by melting, some snow must be present at the beginning of the summer season. It is furthermore shown that the summer runoff in this mountain region is simulated well by the SCN simulation. This indicates that the simulated total snowmelt in this region during summer is realistic. On the other hand, here the DKH and especially the GCM simulations exhibit too little runoff during summer.

There is a large dependence on resolution of the simulated snow depth and of the timing of the snowmelt—the SCN simulation shows much more snow and a later spring melt. Hence, the spring snowmelt is much more pronounced in the high-resolution experiment than in the lower-resolution experiments. Taking into account the underestimation of the observed snow depths, the annual maximum depth simulated by the SCN simulation seems realistic, whereas the DKH and the GCM simulate too little snow. However, it does seem that the SCN simulation has a too late spring melt. This deficiency is explained by the fact that especially the SCN simulation is too cold in all seasons except for the winter. Since the highest mountains are not resolved in the two coarser-resolution simulations the spring melt happens much earlier in these simulations.

3) RUNOFF

We will first illustrate the effect of resolution on the simulated runoff. In Fig. 14 we show the seasonal variation of the monthly mean runoff for the six subregions. There are basically three different types of annual variations.

First, over the low-land areas, where most runoff occurs during autumn and winter and where little or no snow accumulates during winter (subareas DK and SS), the effect of increased resolution is very small. The seasonal variation and main differences between the

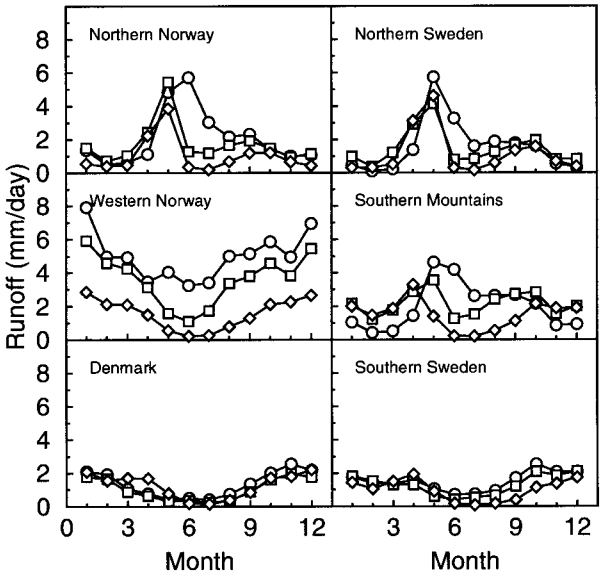

FIG. 14. Average runoff for six subareas of Scandinavia (Fig. 2) and three different simulations (circles: SCN, squares: DKH, diamonds: GCM).

models can be explained by the simulated precipitation amounts (Fig. 11).

Second, in the inner mountain areas and areas with a substantial snowpack during winter (subareas SM, NN, and NS) we notice a delay in the timing of spring melt and an increase in volume with increasing resolution. However, the effect is much stronger going from DKH to SCN than going from GCM to DKH. This must reflect the extreme dependence of snow accumulation and snowmelt timing on the ability to resolve the highest mountains. As noted previously, melting takes place in the SCN simulation also in July (Fig. 13), whereas in the two other simulations snow is practically absent after the beginning of June. The latter is not in accordance with reality.

Finally, in subarea WN, the most rainy part of Scandinavia (see, e.g., Fig. 11), the runoff reflects both an effect of the increase of precipitation and of a delayed snowmelt as a function of increasing resolution. Hence, in the SCN simulation the annual variation in the runoff ends up being rather moderate.

Because of the relatively well simulated summer precipitation (cf. Fig. 11) and the expected better detail in snow distribution, we should expect to see an improvement with higher resolution in the simulated runoff. To illustrate that this is the case, we compare in Fig. 15 the simulated runoff for the three simulations with a similar map of an estimate of the observed runoff (from Raab and Vedin 1995) for the summer season. These maps clearly demonstrate the importance of representing the highest mountains realistically. The GCM simulation is obviously totally unrealistic (no points with a runoff exceeding 50 mm for the season). The pattern of runoff in the DKH simulation is much better, but the amount

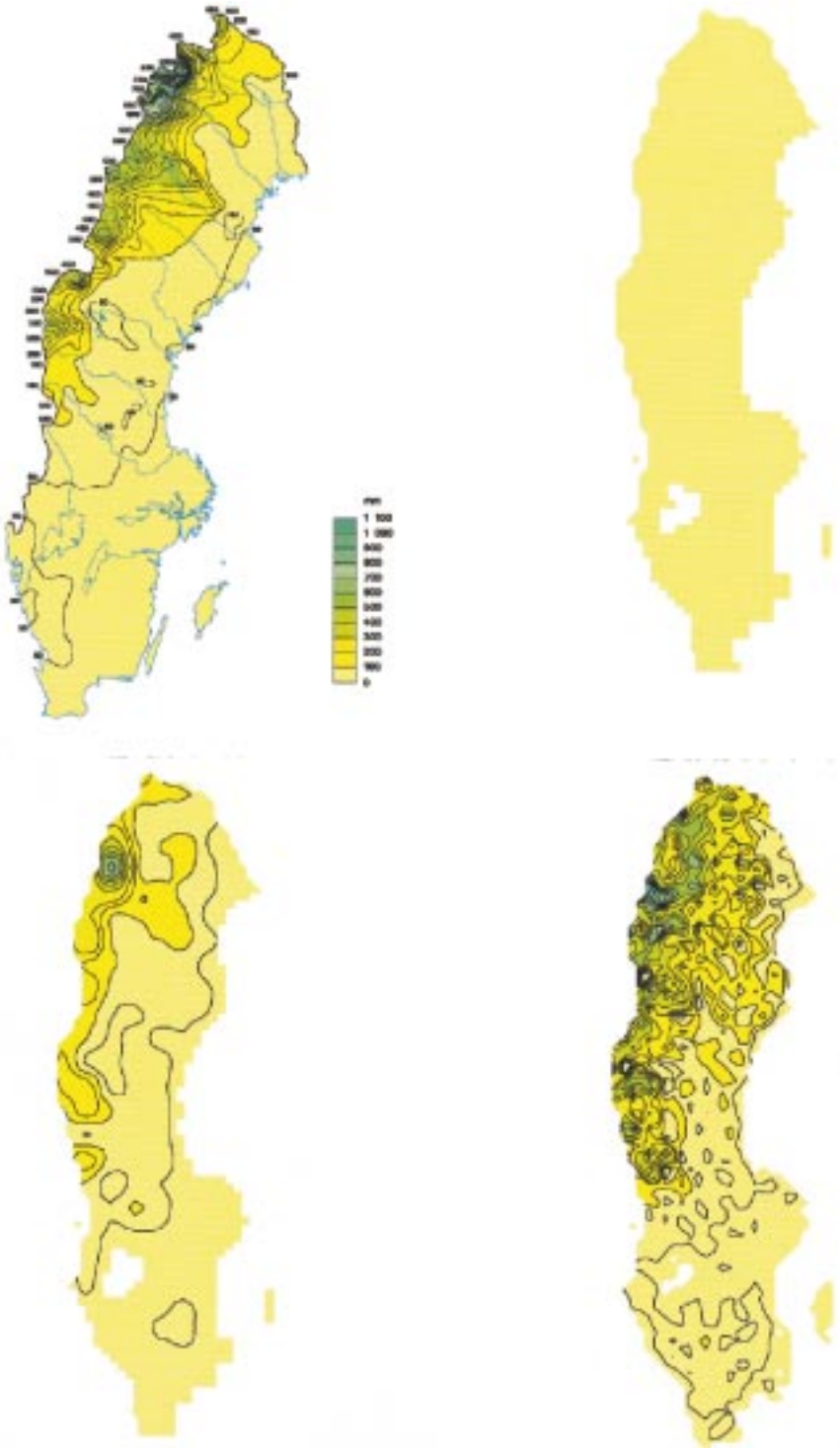

FIG. 15. Summer runoff for Sweden. (upper left) As observed (Raab and Vedin 1995). (upper right) GCM simulation. (lower left) DKH simulation. (lower right) SCN simulation.

of water going into runoff in the high mountains is still underestimated. The pattern simulated in the SCN experiment looks quite realistic.

We have made a more quantitative validation with seasonal area averages in Table 6. Here we have compiled the observed runoff for those of the subareas, which have a part within Sweden. These area-averaged observed runoff values are based on maps from Raab

TABLE 6. Observed and calculated runoff (mm day^{-1}) in Sweden for seasons as well as annual total. The area averages refer to the part of the subareas of Fig. 2 in Sweden.

Season	Source	Northern Norway	Northern Sweden	Southern mountains	Southern Sweden
Winter	Observation	0.5	<0.3	0.3	0.5
	GCM	0.6	0.3	0.9	1.3
	DKH	0.9	0.7	1.3	1.6
	SCN	0.4	0.3	0.5	1.6
Spring	Observation	2.2	1.8	2.5	1.4
	GCM	2.0	2.8	2.6	1.4
	DKH	3.9	2.7	2.6	0.9
	SCN	1.5	2.5	2.1	1.2
Summer	Observation	4.9	1.1	1.2	<0.3
	GCM	0.4	0.3	0.2	0.1
	DKH	3.0	1.0	1.3	0.4
	SCN	4.1	2.2	3.1	0.7
Autumn	Observation	1.8	0.9	0.9	0.8
	GCM	1.2	1.2	1.4	0.8
	DKH	1.9	1.4	2.0	1.4
	SCN	1.0	1.3	1.5	1.8
Total	Observation	2.4	1.0	1.2	0.8
	GCM	1.1	1.2	1.3	0.9
	DKH	2.4	1.5	1.8	1.0
	SCN	1.8	1.6	1.8	1.3

and Vedin (1995) similar to the one in Fig. 15. From Fig. 2 it is evident that the two subareas SM and NN only have relatively few grid points in Sweden on the SCN grid. We do, however, consider them to be sufficiently representative for the two regions.

From Table 6 it is seen that in the high mountains, the Swedish part of subarea NN, the SCN simulation has the most realistic behavior of the annual cycle, although in all seasons with some underestimation, probably because of the spurious accumulation of snow from year to year mentioned above. In the preceding subsection we referred to the results from this area, in particular to the results from the summer season. In this season the observed runoff is 4.9 mm day^{-1}, which is much more than we get in the following conservative estimate of precipitation minus evaporation in this area. The DMI analysis gives a precipitation rate $P = 2.2$ mm day^{-1}, and the CRU analysis gives $P = 2.9$ mm day^{-1}. Allowing for a further increase due to the high wind speed–wetting effect, a conservative estimate of the real value is $P = 3.5$ mm day^{-1}. From this we should subtract the evaporation E. We have no observations available, so we will use the SCN evaporation $E = 0.9$ mm day^{-1}; which should be too small due to the large negative temperature bias in this area (-4.8°C). A resulting estimate is $P - E = 2.6$ mm day^{-1}. This means that the melting must be at least 2.3 mm day^{-1} in order to give the observed 4.9 mm day^{-1} runoff. SCN gives a melting of 2.1 mm day^{-1}, whereas the DKH and GCM simulations give 0.8 mm day^{-1} and a vanishing amount, respectively.

That the SCN melting is too small in the high mountains can also be seen in Fig. 15. We see in this figure that the observed maximum in the runoff coincides with a relative minimum in the simulated runoff in the SCN model. We attribute this discrepancy to the fact that subgrid orographical variability does not enter the expression for surface runoff when snow is present. Hence, since the average surface temperature in the highest mountains is below freezing, the snowmelt actually happening on the mountain slopes and in the local valleys will not take place in the simulation, and snow will accumulate from year to year. In the coarser-resolution simulations the melting can take place due to a lower mean orography. In this connection it should be noted that the surface parameterization in the ECHAM4 model requires the whole snow layer to be above freezing before any snowmelt takes place. These deficiencies in the snow parameterization scheme must be eliminated for high-resolution models.

For the other Swedish subareas it is seen in Table 6 that the simulated summer runoff increases excessively with resolution. The GCM is again giving insufficient runoff, much smaller than observed. The increase from DKH to SCN is due to some melting in NS and SM and in all three subareas increasingly excessive precipitation; furthermore, a large part of the increase is due to a decrease in evaporation explained by the increasingly cold bias with increasing resolution. The increase in melting is connected with the too late spring melt in SCN, which is also influenced by the too low temperatures in SCN.

For the winter season the runoff is small in all subareas. This is captured best in the SCN simulation, except in subarea SS where the effects of too much precipitation and reduced evaporation apparently dominate, giving too high runoff values. In the spring, on the other hand, the SCN runoff is too small in subareas NN, SM, and SS. This must be the result of the too late spring melt, which is dominating the effect of too much precipitation and too little evaporation. The coarser-resolution models simulate more runoff because of their earlier snowmelt. In NS the tendency is the same with decreasing runoff with increasing resolution, but here even the SCN simulation overshoots the observed runoff, as the excessive precipitation and decreased evaporation are not compensated sufficiently by the delayed spring melt. Finally, in the autumn, the runoff in subareas NS, SM, and SS is again larger than observed, which can be explained by uncompensated excessive precipitation and decreased evaporation. Subarea NN is different having the lowest SCN runoff in spite of the largest precipitation and lowest temperatures. The reasons must be the large accumulation of snow in this area due to the deficiencies in the snow parameterization scheme mentioned above and the too low temperature.

4) AN ESTIMATE OF PRECIPITATION MEASUREMENT ERRORS

We have available no direct estimates of how much the analyses of precipitation are underestimating the real

TABLE 7. Details of the estimation of precipitation measurement errors.

	NN	NS	SM	SS
$\Delta E = E_{DKH} - E_{SCN}$ (mm day^{-1})	0.31	0.26	0.29	0.25
$\Delta T = T_{OKH} - T_{SCN}$ (K)	1.60	1.26	1.30	1.19
$\Delta E/\Delta T$	0.19	0.21	0.22	0.21
$\delta T_{DMI} = T_{SCN} - T_{DMI}$	−2.00	−1.47	−1.40	−1.46
$\delta E = \Delta E/\Delta T \times \delta T$ (mm day^{-1})	−0.38	−0.31	−0.31	−0.31
δR (mm day^{-1})	−0.6	0.6	0.6	0.5
δA (mm day^{-1})	0.64	0.03	0.00	0.08
$\delta P = P_{SCN} - P_{true}$ (mm day^{-1})	−0.34	0.32	0.29	0.27
$\delta P_{DMI} = P_{SCN} - P_{DMI}$ (mm day^{-1})	1.43	0.96	1.14	0.89
$P_{corr} = \delta P_{DMI} - \delta P$ (mm day^{-1})	1.77	0.64	0.85	0.62
P_{DMI} (mm day^{-1})	1.84	1.50	1.67	1.78
P_{corr}/P_{DMI}	96%	43%	51%	35%
$\delta P_{DMI}^{CRU} = \delta P_{CRU} - P_{DMI}$ (mm day^{-1})	1.20	0.15	0.26	0.02
$\delta P_{DMI}^{CRU}/P_{DMI}$	65%	10%	16%	1%

precipitation in Norway and Sweden due to wind and wetting effects and an insufficient account of its variation with altitude. As such estimates are essential for the assessment of the model simulation of precipitation we shall try to estimate this indirectly using the observed runoff in the Swedish subareas.

In each subarea we assume a hydrological balance at the surface of annual mean values:

$$P = E + R + A, \tag{3}$$

where R is runoff and A is the rate of accumulation of water in the form of snow and soil moisture. Since we are looking at long-term annual mean values we assume that $A = 0$. Knowing the runoff R we can determine P if the evaporation E can be estimated. Unfortunately no observed fields of E are available, but we can make a reasonable estimate of its bias $\delta E = E_{SCN} - E_{true}$.

The biases must satisfy the balance equation

$$\delta P = \delta E + \delta R + \delta A, \tag{4}$$

where $\delta A = A_{SCN}$ is the spurious accumulation at high mountain peaks in the SCN simulation. The annual mean evaporation and temperature in the DKH and SCN simulations were computed (not shown), and we found that the ratio

$$\frac{\Delta E}{\Delta T} = \frac{E_{DKH} - E_{SCN}}{T_{DKH} - T_{SCN}} \tag{5}$$

is almost equal for the four subareas. The values are shown in Table 7. This fact indicates that the evaporation in the models is approximately a function of the surface temperature T only. This is not unreasonable if the dynamical influence of the wind, surface roughness, and static stability can be assumed to be approximately the same in the models. The main thermodynamic factor that determines evaporation is the actual vapor pressure in the air minus the saturated vapor pressure at the surface temperature, $e_a - e_{sat}(T)$. Assuming this to hold also for time-averaged values, and furthermore that the surface temperature is proportional to the air temperature and a constant relative humidity can be assumed, we get an expression for E approximately proportional to $e_{sat}(T)$.

We now assume that the bias ratio

$$\frac{\delta E}{\delta T} = \frac{E_{SCN} - E_{true}}{T_{SCN} - T_{true}} \tag{6}$$

is equal to the corresponding ratio Eq. (5); that is,

$$\delta E = \frac{\Delta E}{\Delta T}\delta T. \tag{7}$$

In other words, we assume the same temperature dependence of the real evaporation as the evaporation in the models. With these assumptions we can compute the evaporation bias from Eq. (7) using the temperature biases based on the DMI analyses. We have much more confidence in the temperature analyses than in the precipitation analyses, as they have no systematic measurement error and a reasonable variation with altitude has been used in the analyses.

The values of δE obtained are shown in Table 7 as well as the computed values of δR and δA, which were used in Eq. (4) to obtain δP, the ''real'' precipitation biases. The biases δR and δA are also shown in Table 7. Subtracting δP from the corresponding DMI biases $\delta P_{DMI} = P_{SCN} - P_{DMI}$, we get the corrections

$$P_{corr} = P_{true} - P_{DMI} = \delta P_{DMI} - \delta P. \tag{8}$$

As indicated we have listed most steps in the computations in Table 7. We show also the resulting correction values in percent of the DMI analyses. These estimates include effects of both the strong-wind and the wetting errors, and errors due to the altitude dependence of precipitation.

If we accept that the latter effect is taken into account sufficiently well in the CRU analysis, we find that its contribution to the total corrections is as the bottom row of Table 7. As should be expected, the largest corrections are found in the mountain areas, the Swedish part of NN and SM, almost 100% and 50%, respectively, out of which about 30% and 35%, respectively, are due to the wind and wetting effects. For the Swedish part

TABLE 8. Corrected annual precipitation values, CRU analysis bias, and corrected model biases.

	WN	NN	NS	SM	SS	DK
Observation (mm day^{-1})	6.6	4.1	2.1	2.9	2.6	2.4
CRU bias (%)	−24	−32	−25	−19	−27	−16
GCM bias (%)	−51	−48	−7	1	−1	10
DKH bias (%)	−17	−29	17	27	10	7
SCN bias (%)	−1	−20	13	20	8	26

of NS and SS we get total corrections of 43% and 35%, respectively, out of which 33% and 34% should be due to the wind/wetting effects.

Although we have been able to make these estimates for the Swedish part of the subareas only, we shall assume that they are representative for the whole of the subareas. In Table 8 we have used the total correction values listed in Table 7 to correct the annual observed precipitation values and the biases listed in Table 3. For subarea DK we have used the directly estimated values (20%) mentioned earlier, and for WN we have guessed a value of 40%. After these corrections we see that both RCMs have positive biases on the lee side of the Scandinavian mountains and in the DK subarea, but strongly reduced ones compared to the values in Table 3. This is in agreement with what should be expected from the enhanced cyclone activity, which was indicated by the MSLP bias patterns found all year round. On the western side of the mountains, NN gets too dry, also in agreement with the reduced westerlies in this area all year round. Finally, we see in these annual biases the clear improvement with increasing resolution in subarea WN that was pointed out above for most seasons.

6. Summary and conclusions

A 9-yr-long present-day climate simulation has been made with the HIRHAM4 model in 18-km resolution covering Scandinavia (the SCN simulation). In this simulation the model was nested into the same model in a version with 57-km resolution in an area covering Europe (the DKH simulation), which again was nested into the global coupled CGCM, ECHAM4–OPYC. All three model simulations have been verified over Scandinavia against available climatological data.

High-resolution analyses of the 1961–90 climatological mean precipitation and surface air temperature were made using a successive correction method (the DMI analyses). For temperature a close agreement was obtained with the CRU analyses (Hulme et al. 1995) except in certain areas in the north with few observations. For precipitation the analyses were also close except in mountain areas where the higher CRU values are believed to be more accurate due to the direct account of variations with altitude. Due to a denser network of observations over Sweden and Denmark the representation of smaller scales is believed to be improved in the DMI precipitation analysis. The successive correction method was also used to obtain gridded values of snow cover from a coarser resolution dataset. Furthermore, gridpoint values of runoff in Sweden and the frequency of precipitation intensity classes in Norway and Sweden have been obtained by reading off the values from maps in published atlases. From Denmark these data as well as data on cloud cover have been obtained in digital form.

The verification of seasonal mean temperature and precipitation showed significant large-scale biases. For precipitation, however, the uncorrected positive biases in Table 3 should be reduced substantially due to the underestimated analysis values, as indicated by our estimates of corrected annual biases (see Table 8). As in Machenhauer et al. (1998) it was found that these errors to a large extent could be explained by systematic errors in the low-level general circulation and by rather large errors in the SSTs simulated by the CGCM and used in the nested models. For somewhat larger subareas than here, Machenhauer et al. (1998) have shown that the large-scale temperature and precipitation biases are statistically significant compared to estimates of the internal decadal model variability. In other words, the large-scale model biases represent systematic errors and not just sampling errors. Also, it was noted that the large-scale systematic circulation errors, visualized by the MSLP bias pattern, were similar in the three simulations, except for modifications due to the higher resolution in the nested models. This indicates strongly that these errors in the nested models are caused by errors in the imposed boundary fields. Generally the simulated MSLP is too low in a belt across southern Scandinavia, especially in the two RCMs, indicating too strong cyclone activity here with enhanced westerlies to the south of the belt and decreased westerlies to the north of it. This leads generally to enhanced maritime influence south and east of the Scandinavian mountains with increased precipitation and reduced seasonal temperature variations, which are further enhanced due to the SST biases. To the west of the mountain summits the upslope orographic precipitation is clearly improved with increasing resolution because of the more realistic orography, although reduced westerlies tend to reduce the precipitation and the Atlantic thermal influence. The largest changes in the MSLP bias pattern occur between the GCM and the DKH simulation. Generally, the pressure decreases further in the belt of too low pressure, which gives increasing effects on the biases of precipitation and temperature—that is, mostly increasing precipitation and reduced seasonal temperature variation. From the DKH to the SCN simulation the pressure in the belt of too low pressure increases slightly or remains unchanged. This explains small changes, mainly a decrease in precipitation. However, also a large cooling takes place from the DKH to the SCN simulation in all seasons; largest in the summer season, on the average about 1.5°C. In the winter season it can be explained by the changes in the general circulation, but in the other

seasons it cannot. As an explanation it is suggested that especially efficient land–sea breeze systems develop in the very high resolution of the SCN simulation in the warm part of the year, which transport cold air from the surrounding sea.

Concerning the distribution of precipitation intensities, we found that generally the observed distribution is simulated best in the SCN simulation. The models predict too few dry days, but the SCN comes closest to observation with the highest frequency. Also in the large group of medium-intensity precipitation the SCN simulation is best with the fewest occurrences. The simulated frequency of heavy precipitation is found to increase with resolution, and as the observed values are most likely underestimated, it is assumed that also for this intensity class the SCN simulation is the most realistic one. For light precipitation either DKH or SCN come closest to the observed frequency.

Also for the accumulated snowpack the SCN simulation was found to be the most realistic one, apparently with a sufficiently large total accumulated mass and a snowmelt extending into the summer season. The SCN snowmelt seems to occur too late because of the too low temperatures in summer and adjacent seasons, but the other simulations have a too early snowmelt with no melting in summer. The latter is not considered realistic.

The validation of runoff in Sweden showed that the pattern of runoff in the summer season was most realistic in the SCN simulation. In the quantitative subarea validation the SCN simulation was not always found to be the closest to the observed amounts. This was, however, found to be explained by the large-scale biases in temperature and precipitation.

We have demonstrated the importance of resolution for the simulation of the snowpack, accumulating during winter. It is clear that the representation of mountains in a model will play a dominant role for the simulation of the snowpack in a region where the seasonal variation is as pronounced as in Scandinavia. Here the winters are characterized by temperatures well below the freezing point and by a substantial snowpack, in particular in the mountains. The summers are usually warm with temperatures well above freezing. As was clearly seen in Fig. 1 the representation of the Scandinavian mountains is very different in a typical GCM resolution, a typical regional model simulation, and our spatially very detailed regional simulation. The most important point is that with the very high-resolution approach, the major high-altitude areas and mountain ranges are resolved by the model. Even the intermediate-resolution regional model does not resolve the most narrow ridges as in northern Scandinavia, and at the same time underestimates the high peaks and plains in southern Norway. Likewise, the orographic gradients are resolved less accurately, and consequently cause the precipitation from orographic lifting to fall less realistically. This, of course, is even worse with the coarser resolution used in the driving GCM. Hence, for otherwise similarly formulated models, the chance for a good simulation of such regional quantities will deteriorate with decreasing resolution, simply because the relevant mechanisms due to the local geographical properties are less accurately represented.

We have seen that the high-resolution model performs very well given the large-scale forcing by the imposed boundary fields. However, the model performance will always be limited by the quality of these driving fields. Many of the shortcomings in the simulated fields we have presented here are directly linked to systematic errors imposed from the driving GCM (see also Machenhauer et al. 1998). This applies in particular to the too small seasonal amplitude of temperature.

Hence, it is essential for an improved quality of such very high-resolution simulations that the systematic errors in the general circulation over Europe of the driving CGCM are reduced. Also further studies of the mechanisms that lead to increases in the biases with increasing resolution—that is, the supposed enhanced cyclone activity and excessive efficiency of land–sea breeze systems—are needed in order to be able to understand their reason and subsequently to reduce or eliminate them.

Acknowledgments. This research was in part supported by the EC Environment and Climate Research Programme (Contracts EV5V-CT92-0126 and EV5V-CT94-0505, Climate and Natural Hazards). Two of the authors (OBC and JHC) received financial support from ELSAM, the partnership of electricity producers in western Denmark. We thank Ylva Westman of the SMHI for providing the map of observations in Fig. 15 and Povl Frich of the DMI for providing climatological data for Denmark.

REFERENCES

Alexandersson, H., C. Karlström, and S. Larsson-McCann, 1991: Temperature and precipitation in Sweden 1961–1990, reference normals. Swedish Meteorological and Hydrological Institute Rep. 81, 87 pp. [Available from Swedish Meteorological and Hydrological Institute, S-60176 Norköpping, Sweden.]

Allerup, P., and H. Madsen, 1980: Accuracy of point precipitation measurements. *Nordic Hydrol.,* **11,** 57–70.

Aune, B., G. Bjørbæk, and E. Førland, 1993: *National Atlas for Norway.* Norwegian Meteorological Institute and Norwegian Mapping Authority, Maps 3.1.2, 3.1.3, and 3.1.6.

Bergthorsson, P., and B. Doos, 1955: Numerical weather map analysis. *Tellus,* **7,** 329–340.

Blackmon, M. L., 1976: A climatological spectral study of the 500 mb geopotential height of the Northern Hemisphere. *J. Atmos. Sci.,* **33,** 1607–1623.

Christensen, J. H., O. B. Christensen, P. Lopez, E. van Meijgaard, and M. Botzet, 1996: The HIRHAM4 regional atmospheric climate model. Scientific Report 96-4, Danish Meteorological Institute, 51 pp. [Available from Danish Meteorological Institute, Lyngbyvej 100, DK-2100 Copenhagen Ø, Denmark.]

——, B. Machenhauer, R. G. Jones, C. Schär, P. M. Ruti, M. Castro, and G. Visconti, 1997: Validation of present-day regional climate simulations over Europe: LAM simulations with observed boundary conditions. *Climate Dyn.,* **13,** 489–506.

Claussen, M., U. Lohmann, E. Roeckner, and U. Schulzweida, 1994: A global data set of land-surface parameters. MPI Report 135, Max-Planck Institut für Meteorologie, 30 pp. [Available from Max-Planck-Institut für Meteorologie, Bundesstr. 55, D-20146 Hamburg, Germany.]

DNMI, 1994: Klimatologisk månedsoversikt. Norwegian Meteorological Institute Rep. [Available from Norwegian Meteorological Institute, P.O. Box 43, Blindern, N-0313 Oslo, Norway.]

Dümenil, L., and E. Todini, 1988: A rainfall-runoff scheme for use in the Hamburg climate model. *Advances in Theoretical Hydrology.* Vol. 1, EGS Series of Hydrological Sciences, Elsevier, 129–157.

Foster, D. J., and D. R. Davy, 1988: Global snow depth climatology. Publ. AFETAC/TN-88/006, U.S. Air Force, 48 pp.

Gates, W. L., 1992: AMIP: The atmospheric model intercomparison project. *Bull. Amer. Meteor. Soc.,* **73,** 35–62.

Giorgetta, M., and M. Wild, 1996: The water vapour continuum and its representation in ECHAM4. MPI Rep. 162, Max-Planck-Institut für Meteorologie, 38 pp. [Available from Max-Planck-Institut für Meteorologie, Bundesstr. 55, D-20146 Hamburg, Germany.]

Giorgi, F., 1990: Simulation of regional climate using a limited area model nested in a general circulation model. *J. Climate,* **3,** 941–963.

——, and L. O. Mearns, 1991: Approaches to the simulation of regional climate change: A review. *Rev. Geophys.,* **29,** 191–216.

Hulme, M., D. Conway, P. D. Jones, T. Jiang, E. M. Barrow, and C. Turney, 1995: Construction of a 1961–1990 European climatology for climate change modeling and impact applications. *Int. J. Climatol.,* **15,** 1333–1363.

Jäger, L., 1983: Monthly and areal patterns of mean global precipitation. *Variations in the Global Water Budget,* S.-P. Alayne, Ed., Reidel, 129–140.

Jones, R. G., J. M. Murphy, and M. Noguer, 1995: Simulation of climate change over Europe using a nested regional climate model. Part I: Assessment of control climate including sensitivity to location of lateral boundaries. *Quart. J. Roy. Meteor. Soc.*, **121,** 1413–1449.

Källberg, P., and R. Gibson, 1977: Multi level limited area forecasting using boundary zone relaxation. GARP Programme on Numerical Experimentation, Rep. 15, 128 pp.

Källén, E., Ed., 1996: HIRLAM documentation manual, system 2.5. Swedish Meteorological and Hydrological Institute, 126 pp. [Available from SMHI, S-60176 Norrköping, Sweden.]

Legates, D. R., and C. J. Willmott, 1990: Mean seasonal and spatial variability in gauge-corrected global precipitation. *Int. J. Climatol.,* **10,** 111–127.

Machenhauer, B., M. Windelband, M. Botzet, R. G. Jones, and M. Déqué, 1996: Validation of present-day regional climate simulations over Europe: Nested LAM and variable resolution global model simulations with observed mixed layer ocean boundary conditions. MPI Rep. 191, Max-Planck-Institut für Meteorologie, 60 pp. [Available from Max-Planck-Institut für Meteorologie, Bundesstr. 55, D-20146 Hamburg, Germany.]

——, ——, ——, J. H. Christensen, M. Déqué, R. G. Jones, P. M. Ruti, and G. Visconti, 1998: Validation and analysis of regional present-day climate and climate change simulations over Europe. MPI Rep. 275, Max-Planck-Institut für Meteorologie, 80 pp. [Available from Max-Planck-Institut für Meteorologie, Bundesstr. 55, D-20146 Hamburg, Germany.]

Mearns, L. O., F. Giorgi, L. McDaniel, and C. Shields, 1995: Analysis of the variability of daily precipitation in a nested modeling experiment: Comparison with observation and 2 × CO results. *Global Planet. Change,* **10,** 55–78.

Morcrette, J.-J., 1991: Radiation and cloud radiative properties in the ECMWF forecasting system. *J. Geophys. Res.,* **96,** 9121–9132.

Nordeng, T. E., 1994: Extended versions of the convective parameterization scheme at ECMWF and their impact on the mean and transient activity of the model in the Tropics. ECMWF Rep. 206, ECMWF, 41 pp. [Available from European Centre for Medium-Range Weather Forecasts, Shinfield Park, Reading, Berkshire RG2 9AX, United Kingdom.]

Oberhuber, J. M., 1992: The OPYC Ocean General Circulation Model. DKRZ Rep. 7, DKRZ, 127 pp. [Available from Deutsches Klimarechenzentrum GMbH, Bundesstr. 55, D-20146 Hamburg, Germany.]

——, 1993: Simulation of the Atlantic circulation with a coupled sea ice–mixed layer–isopycnal general circulation model. Part I: Model description. *J. Phys. Oceanogr.,* **22,** 808–829.

Olson, J. S., J. A. Watts, and L. J. Allison, 1983: Carbon in live vegetation of major world ecosystems. ORNL-5862, Oak Ridge Laboratory. [Available from Oak Ridge National Laboratory, Oak Ridge, TN 37831.]

Raab, B., and H. Vedin, Eds., 1995: *Climate, Lakes and Rivers: National Atlas for Sweden.* SNA Publishing, 176 pp. and 198 plates.

Roeckner, E., and Coauthors, 1992: Simulation of the present-day climate with the ECHAM model: Impact of model physics and resolution. MPI Rep. 93, Max-Planck-Institut für Meteorologie, 172 pp. [Available from Max-Planck-Institut für Meteorologie, Bundesstr. 55, D-20146 Hamburg, Germany.]

——, J. M. Oberhuber, A. Bacher, M. Christoph, and I. Kirchner, 1996a: ENSO variability and atmospheric response in a global coupled atmosphere-ocean GCM. *Climate Dyn.,* **12,** 737–754.

——, and Coauthors, 1996b: The atmospheric general circulation model ECHAM-4: Model description and simulation of present-day climate. MPI Rep. 218, Max-Planck-Institut für Meteorologie, 90 pp. [Available from Max-Planck-Institut für Meteorologie, Bundesstr. 55, D-20146 Hamburg, Germany.]

Sass, B. H., 1994: The DMI operational HIRLAM forecasting system version 2.3—A short summary. DMI Rep. 94-8, Danish Meteorological Institute, 10 pp. [Available from Danish Meteorological Institute, Lyngbyvej 100, DK-2100 Copenhagen Ø, Denmark.]

Shapiro, R., 1970: Smoothing, filtering and boundary effects. *Rev. Geophys. Space Phys.,* **8,** 359–387.

Sundqvist, H., 1988: Parameterization of condensation and associated clouds for weather prediction and general circulation simulations. *Physically-Based Modeling and Simulation of Climate and Climate Change,* M. E. Schlesinger, Ed., Reidel, 433–461.

Tiedtke, M., 1989: A comprehensive mass flux scheme for cumulus parameterization in large-scale models. *Mon. Wea. Rev.,* **117,** 1779–1800.

Vejen, F., 1996: An operational system for correcting precipitation for the aerodynamic effect (in Danish). *Proceedings of the Nordic Hydrological Conference 1996,* Vol. 1, Akureyri, Iceland, NHP Rep. 40, 263–272.

Williamson, D. L., and P. J. Rasch, 1994: Water vapor transport in the NCAR CCM2. *Tellus,* **46A,** 34–51.